

Research papers

Characterising the coincidence of soil moisture – precipitation extremes as a possible precursor to European floods

Ashish Manoj J^{a,b,c,d,*}, Teresa Pérez Ciria^{b,e}, Gabriele Chiogna^b, Nadine Salzmann^{f,g}, Ankit Agarwal^{a,h}

^a Department of Hydrology, Indian Institute of Technology Roorkee, Roorkee 247667, India

^b Chair of Hydrology and River Basin Management, Technical University of Munich, Arcistr. 21, 80333 Munich, Germany

^c Department of Geosciences, University of Fribourg, 1700 Fribourg, Switzerland

^d Institute of Water and River Basin Management – Hydrology, Karlsruhe Institute of Technology, Kaiserstr. 12, 76131 Karlsruhe, Germany

^e Department of Geography, Ludwig-Maximilians-Universität München (LMU), Luisenstr. 37, 80333, Munich, Germany

^f WSL Institute for Snow and Avalanche Research SLF, Flüelastrasse 11, 7260 Davos Dorf, Switzerland

^g Climate Change, Extremes and Natural Hazards in Alpine Regions Research Center CERC, Flüelastrasse 11, 7260 Davos Dorf, Switzerland

^h Section 4.4: Hydrology, GFZ German Research Centre for Geosciences, Potsdam 14473, Germany

ARTICLE INFO

This manuscript was handled by Andras Barossy, Editor-in-Chief, with the assistance of Roger Moussa, Associate Editor

Keywords:

Soil moisture

Floods

ECA

SM-P coupling

Europe

ABSTRACT

Studies around the world have shown that increases in extreme precipitation are not directly resulting in reported instances of flooding. Despite the evidence that antecedent soil moisture conditions play a significant role in regulating the runoff response during extreme storm events, fewer works have tried to understand the spatial and temporal dynamics of such coupled interactions. In the present work, we aim to improve our understanding of the dominant spatiotemporal patterns of soil moisture (SM) – precipitation (P) dependence over Europe. Using an event-based, non-parametric Event Coincidence Analysis (ECA) approach, we first quantified the probability of SM preceding P by the precursor coincidence rate. We also examined the statistical precursor relationship between SM-P joint episodes and reported annual flood events using the conditional precursor coincidence rate. The results show that seasonality is a major driving force in the spatiotemporal dynamics of SM-P coupling over Europe. The conditional precursor coincidence rates are in line with previous flood hazard studies over Europe and show the importance of considering such diverse interdependencies in flood risk mitigation. Our work has implications for understanding the occurrence of preconditioned compound events worldwide and provides a vital starting point for characterising the major processes that need to be accounted for in comprehensive state of the art flood risk assessment studies.

1. Introduction

Globally, floods are considered one of the most devastating and prevalent natural hazards impacting regions across continents and various diverse climatic regimes (Coumou and Rahmstorf, 2012; Merz et al., 2021; Seneviratne et al., 2021). The marked shifts in the global water cycle due to climatic variability and anthropogenic forcings are nowadays becoming more common and widespread (IPCC, 2021). Furthermore, anthropogenic climate change coupled with socio-economic shifts in population exposure is expected to play a major role in shaping future flood hazard risk (Gu et al., 2020; Kam et al., 2021). Even

though the risk of catastrophic flooding has impacted Europe throughout history (Barredo, 2007; Brázdil et al., 2006), human-induced alterations in the global earth system have led to significant changes in the patterns and intensity of flooding events in Europe (Bertola et al., 2021; Blöschl et al., 2017; Madsen et al., 2014). This is further expected to result in a substantial increase in future flood damages (Alfieri et al., 2015; Dottori et al., 2023; Jongman et al., 2014). These facts call for a better understanding of the predominant flood risk patterns over Europe.

Extreme precipitation events have increased over the past few decades (Papalexiou and Montanari, 2019; Westra et al., 2013).

* Corresponding author (Currently at: Institute of Water and River Basin Management – Hydrology, Karlsruhe Institute of Technology, Kaiserstr. 12, 76131 Karlsruhe, Germany).

E-mail addresses: ashish_m@hy.iitr.ac.in, ashish.jaseetha@kit.edu (A. Manoj J), teperez.ciria@tum.de (T. Pérez Ciria), gabriele.chiogna@tum.de (G. Chiogna), nadine.salzmann@slf.ch (N. Salzmann), ankit.agarwal@hy.iitr.ac.in (A. Agarwal).

<https://doi.org/10.1016/j.jhydrol.2023.129445>

Received 1 September 2022; Received in revised form 13 February 2023; Accepted 23 March 2023

Available online 27 March 2023

0022-1694/© 2023 Elsevier B.V. All rights reserved.

Precipitation extremes are controlled by both thermodynamic (local exchanges in heat, moisture, and other related quantities) and dynamic processes (those related to atmospheric and oceanic motions/teleconnections) at the regional scale. Recent studies (Seneviratne et al., 2021) have reported that the observed rate of increased precipitation extremes at the global scale, are in line with the famous Clausius-Clapeyron relation (Pall et al., 2007). The role of predecessor rain events in generating peak discharge has already been established globally (Bischniotis et al., 2018; Froidevaux et al., 2015). However, the global increase in precipitation extremes has not directly translated into a rise in reported flood events (Do et al., 2017). Flood initiation and magnitude are invariably impacted by the intensity of precipitation, landform, land use land cover change, soil properties and antecedent catchment conditions, including soil moisture and snowpack. Previous studies have found that the decrease in antecedent soil moisture has led to a decline in observed flood discharge even with increased extreme precipitation (Sharma et al., 2018; Wasko et al., 2020; Wasko and Nathan, 2019). Soil moisture also plays a vital role in water and energy budget equations through its impact on evapotranspiration (Seneviratne et al., 2010). It also partitions the rainfall into various other hydrological cycle components – evapotranspiration, infiltration and runoff, and hence directly impacts flood characteristics (Hlavcova et al., 2005; Komma et al., 2008; Massari et al., 2018; Zehe and Blöschl, 2004; Zhai et al., 2018).

The interaction between antecedent catchment wetness and precipitation can be critical in shaping the runoff response. However, traditional risk assessment approaches usually only focused on univariate (precipitation/peak flood discharge) modelling techniques to study the flood characteristics. Several studies around the world have now shown that univariate approaches underestimate the risk of an extreme event (Leonard et al., 2014; Zscheischler et al., 2018; Zscheischler and Seneviratne, 2017) and that most natural hazards are caused by a combination of multiple statistically dependent physical processes arising across multiple spatial and temporal scales (Kemter et al., 2021; Zscheischler et al., 2020). The IPCC Special Report on Climate Extremes (SREX-2012; Seneviratne et al., 2012) first defined this broad class of events as “compound events”. Specifically, preconditioned compound events are events in which an underlying weather-driven or climate-driven precondition leads to an alteration, generally an increase, in the impacts of a hazard (Bevacqua et al., 2021; Zscheischler et al., 2020). It is also worthwhile to note here that the existing precondition could also have an attenuating/stabilising effect and reduce the impact of the subsequent hazard like in the case of dryer antecedent conditions before floods (Blöschl et al., 2017).

The importance of such initial hydrologic conditions on catchment response cannot be overemphasised (Garg and Mishra, 2019; Khatun et al., 2022). Berghuijs et al. (2019b) illustrated the importance of such conditions over European catchments and they showed that most annual peak floods in Europe are caused not by large precipitation events but by the mutual co-occurrence or coincidence of rainfall with either snowmelt or soil saturated conditions. Ghajarnia et al. (2020) demonstrated the close statistical covariation relationship between soil moisture and runoff anomalies for the different European climatic regimes. Using a data-driven multi-catchment comparative approach with different datasets, they unravelled a dominant first-order covariation between soil moisture and runoff on the monthly scale. Blöschl et al. (2017) analysed the timing of river floods in Europe from 1960 – to 2010 and found a clear shift in the timings of winter floods over western Europe due to earlier soil moisture maxima. Wasko et al. (2021) examined the trends in streamflow using a global dataset and attributed the decreasing trend of frequent flood magnitudes to the dominance of drying antecedent soil moisture conditions in contrast to the intensification of short-duration precipitation. Grillakis et al. (2016) compared the importance of initial soil moisture conditions for flash flood generation over different catchments and found that the peak discharge was dependent on soil moisture states, and the magnitude of the impact relies on the

magnitude of the event. However, within the available literature, studies attempting to contextualize the Soil Moisture (SM) – Precipitation (P) preconditioning at a European scale is particularly sparse and very few works have attempted to understand the changing regional patterns between such SM-P relationships at a seasonal scale. Hence, there is a growing need to account for the role played by antecedent catchment wetness before a precipitation event in shaping the catchment response and their seasonal changes. Specifically, it becomes necessary to characterise the spatiotemporal patterns of coincidence between Soil Moisture (SM) and Precipitation (P) events. The benefits of establishing such spatial information maps in the context of flood hydrology (Merz and Blöschl, 2008) and in characterising hydroclimatic covariability (Sun et al., 2018) are already well established in the literature. The seasonal changes in such patterns could further aid in understanding how the different climatic regions of Europe behave in the context of SM-P covariability.

Traditional measures like correlation and covariance are indeed helpful in understanding the spatiotemporal patterns of SM-P dependence. However, the interdependencies are evaluated considering the entire distribution of data. They describe dependence at the centre of the distribution and may under/overestimate dependence in the joint tails of the distribution (Jiang et al., 2020; Siegmund et al., 2016b). Some more commonly used linear methods may fail when the underlying distributions exhibit significant deviations from the Gaussian assumption. Analyses involving identifying and subsequently extracting discrete events (of interest) from a continuous-time series are common in hydrological sciences. From an observed streamflow record at a gauging site, only a few specified high discharge events are usually considered for flood frequency analysis. (Adamowski et al., 1998; Bezak et al., 2014; Taesombut and Yevjevich, 1978).

Event Coincidence Analysis (ECA; Donges et al., 2016) is a non-parametric statistical tool that has received considerable attention in the past few years. Previous work across many diverse scientific disciplines has shown that ECA can characterise the statistical interdependencies between different variables/processes in many varied settings (Christopoulos et al., 2020; Fdez-Arroyabe et al., 2020; Tempel et al., 2021; Wiedermann et al., 2021). Furthermore, a statistical significance test checks the robustness of the obtained coincidence rates (Donges et al., 2016; Siegmund et al., 2017).

However, only a few studies have employed ECA to characterise the spatial and temporal dynamics of SM-P coupling. Sun et al. (2018) was the first to illustrate the spatiotemporal patterns of SM-P coupling using the ECA approach. They characterised the spatial patterns for Texas in the US and further linked the results with the dominant seasonal climatology of the study region. Manoj et al. (2022) evaluated the spatiotemporal dependence between SM and P across India using ECA and additionally investigated their temporal evolution over time and compared it with the changing behaviour of precipitation during the same duration. The previous works considered two variables (SM&P) to quantify the SM-P coincidence rates and infer the dynamics of their changing spatiotemporal patterns. The basic two-variable ECA can also be advanced to account for the role of a third observable/process (Siegmund et al., 2016a). Such a Conditional Event Coincidence Analysis (CECA; Siegmund et al., 2016a) could help in additionally considering the conditioning of events on instances governed by a third variable. To the best of our knowledge, no previous work has attempted to incorporate discharge as a third variable in the ECA framework to statistically quantify the role of SM-P coincidences as a possible precursor to the annual flood events. Such an analysis would offer additional information on the lagged dependence of annual floods on soil moisture – precipitation preconditioning.

Advancing our understanding of soil moisture (SM) – precipitation (P) interactions would help in robustly characterising the regions over which a dominant statistical dependence exists between SM and P. Identifying areas/catchments which experience a co-occurrence/coincidence between SM and P anomalies can be considered critical

for better understanding the occurrence and propagation of large-scale flood events like the one of July-2021 in Western Europe (Dietze et al., 2022; Ibebuchi, 2022). The timing of annual peak floods could also be used to investigate such SM-P coincidences prior to the annual flood events over different European climatic regions. With this motivation, in the present work, we: a) describe the spatiotemporal patterns of SM-P coincidence over Europe and then try to visualise the changing seasonal nature of such SM-P dependence over the different climatic regions b) identify and contextualise the annual floods occurring after such SM-P coincidences have already taken place.

The article is organised as follows: Section 2 briefly introduces the study area and datasets used for the analysis. The steps used in data preparation and a summary of Event Coincidence Analysis are presented in Section 3. Section 4 details the results of the present study, and Section 5 the discussions. Final concluding remarks are provided in Section 6.

2. Study area & data

2.1. Study area

Understanding the possible role of antecedent conditions for floods is vital for setting up reliable flood estimation and forecast mechanisms at the European scale. Previous studies have shown that the mean annual timing of floods over Europe is spatially well defined with distinct regional differences for their seasonality and generation mechanism. The dominant flood generation mechanisms include precipitation excess, soil moisture excess and snowmelt driven floods (Berghuijs et al., 2019b; Blöschl et al., 2019, 2017; Hall and Blöschl, 2018). Below 60° latitude, annual floods are typically seen in parts of western Europe in winter and transition to spring floods in the east. Above 60° latitude, except for coastal areas, spring floods are more widespread. The interplay between catchment conditions (e.g., soil saturation due to persistent rainfall events) and precipitation events often leads to a catchment response quite different from the ones expected due to the precipitation events acting alone. This is particularly important to characterise from an extreme event perspective (Merz et al., 2021). Indeed, in the near past, intense flooding episodes have been caused by extreme precipitation and moderate catchment wetness (Blöschl et al., 2007) and by moderate precipitation and extreme catchment wetness conditions (Schröter et al., 2015). The Köppen-Geiger climate classification zones for Europe include - cold semi-arid climate (BSk), hot summer Mediterranean climate (Csa), warm summer Mediterranean climate (Csb), humid subtropical climate (Cfa), cold desert climate (BWk), hot desert climate (BWh), hot semi-arid climate (BSh), warm dry summer continental climate (Dsb), temperate maritime climate (Cfb) and warm summer humid continental climate (Dfb) (Peel et al., 2007).

The IPCC – SREX, 2012, classified the climatic zones into three distinct classes - Northern Europe (NEU), Central Europe (CEU), and Southern Europe (SEU). The climatic homogeneity was characterised by mean states of precipitation and temperature considering Köppen-Geiger climatic regions and the annual precipitation cycle. In the latest AR6 assessment of the IPCC, the classification system was further refined to better represent consistent regional climate features; however, the spatial boundaries of the three major European regions from SREX-2012 – NEU, CEU and SEU have been maintained unaltered since they encompass the main regional climates in Europe (Iturbide et al., 2020). Within Europe, the transition of climate types from west to east due to continentality and its subsequent impacts are already well documented in literature (Grabowska, 2008; Mikolaskova, 2009; Moghim et al., 2022; Thompson, 1995). The mean annual timings of floods over Europe also exhibit a west to east transition (Hall and Blöschl, 2018). To account for the impact of such a west to east gradient on the seasonal evolution of SM-P coincidence rates within the three IPCC-SREX regions, we subdivided each region into two based on the 15°E longitude. They are conveniently classified as – West NEU, East NEU,

West CEU, East CEU, West SEU, and East SEU.

In the present work, the analysis is being carried out at a grid scale, and we then compare and interpret our results based on the homogenous regions classification. Fig. 1 details the six major regions covered.

2.2. Data

E-OBS (v24.0: Cornes et al., 2018) grid-based daily precipitation product was used in the current study. The final time series is obtained from the station network of the European Climate Assessment & Dataset (ECA&D) project. E-OBS is a pan-European continental-scale observational dataset of several surface climate variables, including daily precipitation, mean, maximum and minimum temperatures. The dataset is based on observations from meteorological stations spanning across Europe provided by the National Meteorological and Hydrological Services (NMHSs) and other relevant data holding institutes (Klein Tank et al., 2002). It is an ensemble dataset constructed through a conditional simulation approach (Cornes et al., 2018; Klein Tank et al., 2002; Klok and Klein Tank, 2009). Previous works have assessed the ability of E-OBS to replicate the observed precipitation characteristics over Europe and have reported encouraging results (Bandhauer et al., 2022; Hu and Franzke, 2020; Kostopoulou et al., 2012). The E-OBS product has also been extensively used over Europe in flood hazard assessment studies (Berghuijs et al., 2019b, 2019a; Blöschl et al., 2019, 2017). The spatial resolution of the precipitation product used here is 0.25° x 0.25°. The monthly climatology of mean daily precipitation for the six regions is depicted in Fig. 2.

The modelled soil moisture product used in the present work comes from the GLEAM (v3.5 Martens et al., 2017) model. GLEAM stands for Global Land Evaporation Amsterdam Model (Martens et al., 2017; Miralles et al., 2011). It is worthwhile to point out that the best possible way to characterise the SM-P spatiotemporal patterns would be by using observational datasets for both Soil Moisture and Precipitation. However, no continental-scale observational dataset exists for soil moisture with consistent and homogenous spatial and temporal coverage. Hence there is a need to use alternate datasets for this purpose. The GLEAM model product used here has been previously used to study the spatio-temporal dynamics of the water cycle and for characterising extreme events (Alsafadi et al., 2022; Ghajarnia et al., 2020; Good et al., 2017; Guillod et al., 2015; Miralles et al., 2014; Pyrali et al., 2022; Schumacher et al., 2019). The soil moisture product was also available at a daily temporal scale with a spatial resolution of 0.25° x 0.25°. Fig. 3 shows the monthly changes in soil moisture across the different hydro-climatic regions considered in the present work.

The discharge peaks were taken from the European Flood Database (Fig. 1: Blöschl et al., 2017; Hall et al., 2015; Hall and Blöschl, 2018), consisting of the day of occurrence of annual maximum discharge values or water levels (daily or instantaneous values). The dataset is available for 4062 catchments over Europe. Similar to Berghuijs et al. (2019b), we do not consider the catchments over Iceland in the present work. The outlet elevations range from around sea level to almost 2000 m, with the catchment area ranging from 10 to 100000 km² (Hall et al., 2015; Hall and Blöschl, 2018). To compare the dates of annual flows with SM-P coincidences, we compare the flood events with the SM and P events for the grid cell where the streamflow gauging station is located. Flood generation is usually produced over the entire catchment area. Nevertheless, with this simplification we are able to obtain a first estimate of the catchments where significant dependence exists between SM-P coincidences and the peak discharge events. This limitation is discussed in more detail in Section 5.4.

3. Methodology

In the present section, we first explain briefly the steps involved in data preparation (3.1); we then detail the Event Coincidence Analysis (ECA) in (3.2) used in (4.1) for unravelling the seasonal SM-P

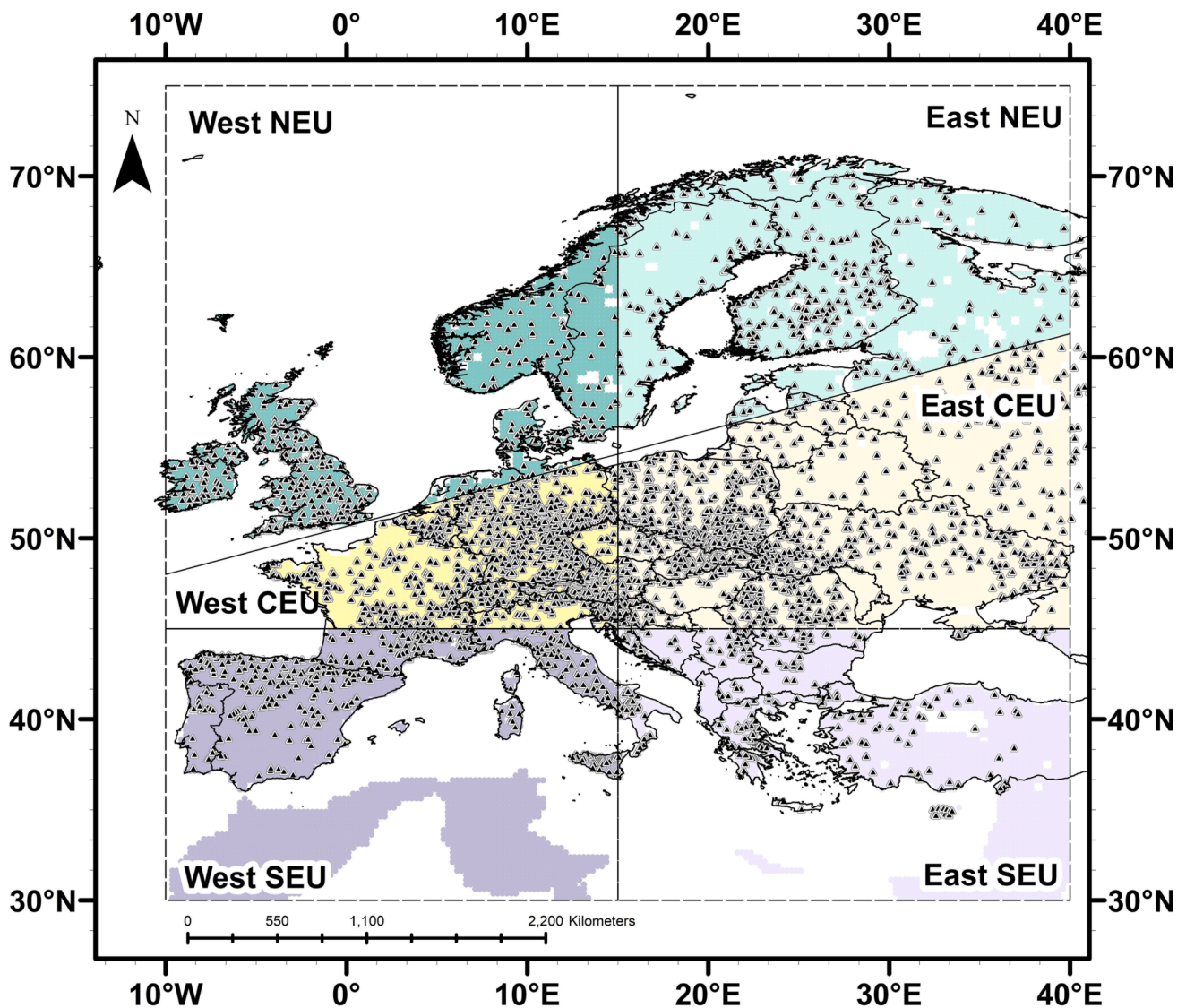


Fig. 1. The six major regions – West NEU, East NEU, West CEU, East CEU, West SEU, and East SEU, referred to in the study, with the location of grid points used for characterising the SM-P coincidence relationship over Europe. Also shown are the location of the catchment outlets from [Hall et al., 2015](#), used for comparing the dates of annual floods with SM-P coincidences.

coincidences over the major European climatic regions, followed by Conditional Event Coincidence Analysis in (3.3) used in (4.2) for comparing the dates of annual peak floods over European catchments with the SM-P coincidences.

3.1. Data Pre-processing

The E-OBS precipitation product was retrieved from the Copernicus Climate Change Service website. The GLEAM product was accessed via the GLEAM project's official website. The discharge data was downloaded from the Ingenieurhydrologie und Wassermengenwirtschaft, TU Wien website (Links to data are provided in the [data availability statement](#)). Precipitation and Soil Moisture products had a spatial resolution of $0.25^\circ \times 0.25^\circ$; however the spatial overlaps were different, and hence bilinear spatial remapping technique ([Schulzweida, 2019](#)) was used to interpolate the GLEAM product to the E-OBS grid. Similar to [Sun et al. \(2018\)](#) and [Manoj et al. \(2022\)](#), we use the daily time step to characterise the SM-P dependence patterns. To disentangle the SM-P coincidences at a seasonal scale, the daily time series corresponding to every grid point is split into four seasons, Winter (DJF), Spring (MAM), Summer (JJA) and Fall (SON). We identify the top 5% events for

Precipitation and Soil Moisture for each season at each grid point using the respective seasonal 95th percentile limit (which on average, leads to about 185–189 events in total per season for both P and SM). This is widely adopted in a number of studies for defining extreme events ([Leckebusch and Ulbrich, 2004](#); [Manoj et al., 2022](#); [Mondal et al., 2020](#); [Pendergrass, 2018](#); [Sheridan and Lee, 2018](#)). The event series is finally represented as a binary series (0 and 1) in which 1 denotes the presence of an event and 0 denotes the absence of an event during a timestep. Figs. C1 and C2 in Appendix-C [Supplementary Information](#) shows the spatial map of the percentile cutoffs used for Precipitation and Soil Moisture respectively.

For the discharge dataset, the peak flood events are compared with the precipitation and soil moisture events for the grid cell where the streamflow gauging station is located. To maintain temporal overlap between the products, the SM-P dependence patterns are evaluated at a seasonal scale from 1980 to 2020. Due to the temporal coverage of the flood discharge data, flood peaks are compared for the period from 1980 up to 2010 only. To ensure a sufficient sample size for each season, the flood analysis is always restricted to catchments having more than five events. In conjunction with the statistical significance test, this ensures that our results are significant and not subject to random effects.

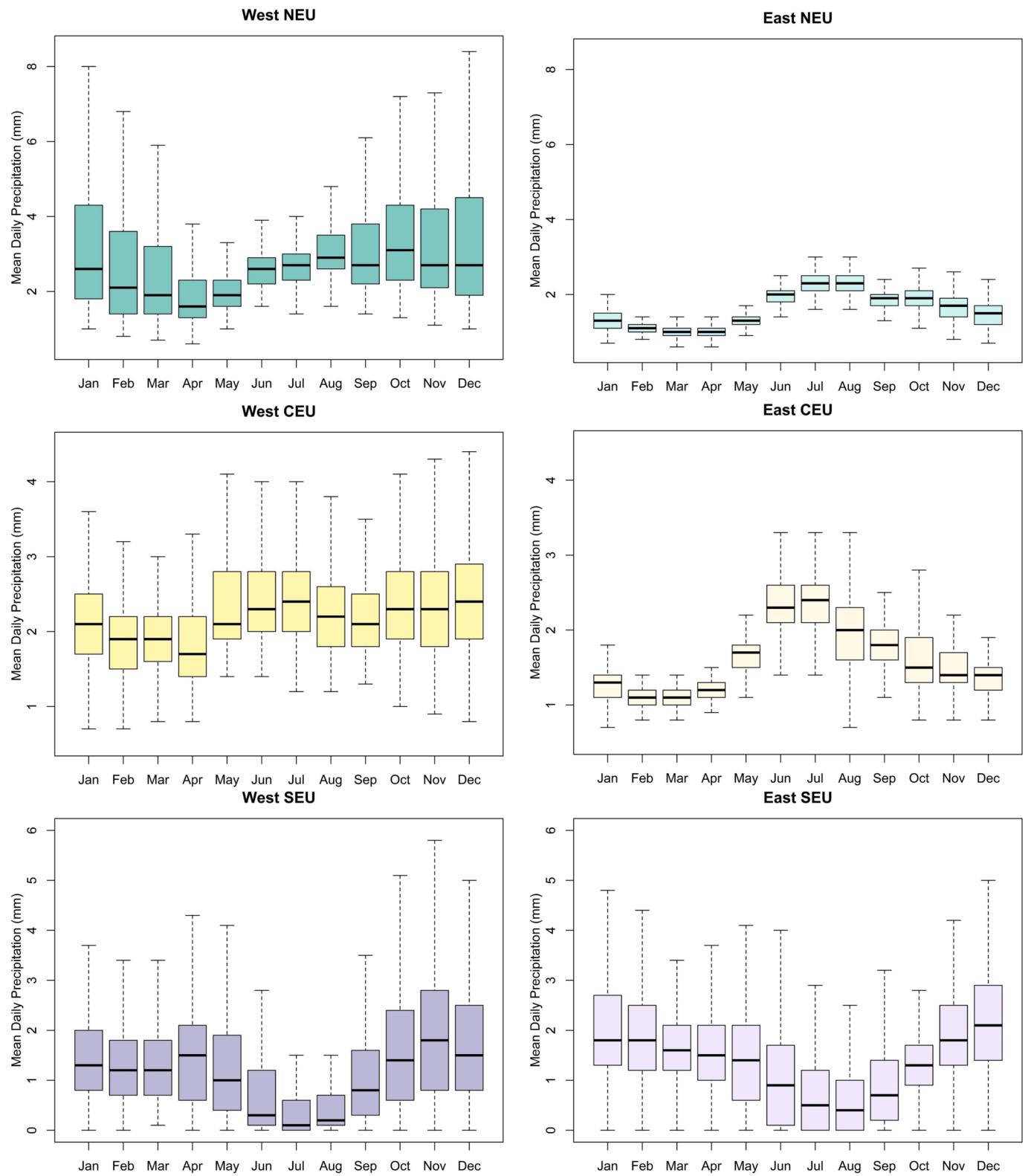


Fig. 2. Boxplots showing the monthly variations in mean daily precipitation (mm) for the six hydroclimatic regions considered in the present work – West NEU, East NEU, West CEU, East CEU, West SEU, East SEU. (Outliers are not shown).

Table D1 in [Supplementary Information](#) details the number of flood events considered per season for each catchment.

3.2. Event coincidence analysis (ECA)

Event Coincidence Analysis (ECA) ([Donges et al., 2016, 2011](#); [Siegmund et al., 2017](#)), is a statistical, non-parametric method used to quantify and characterise the coincidence rates between two sequences

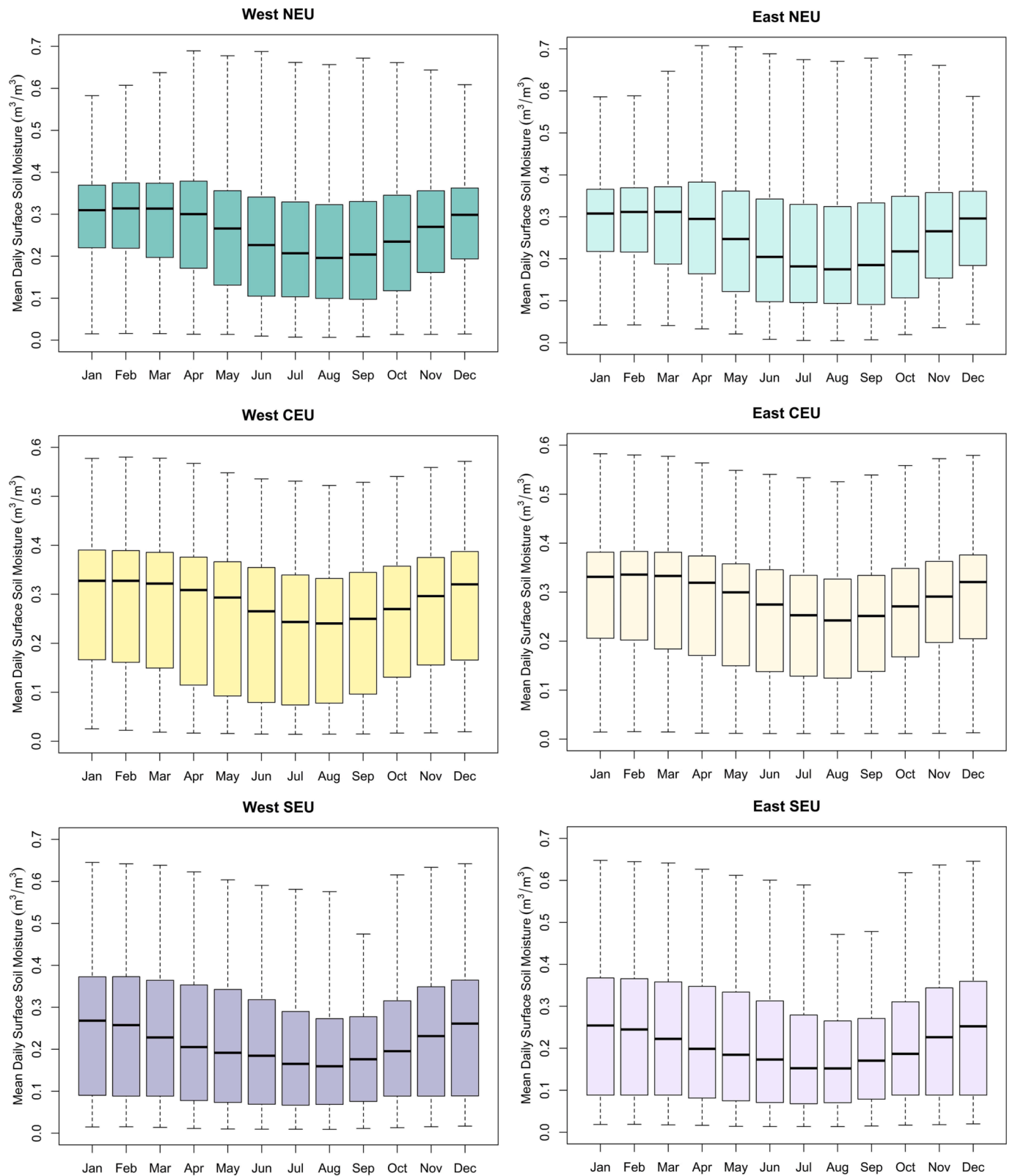


Fig. 3. Boxplots showing the monthly variations in surface soil moisture (m^3/m^3) for the six hydroclimatic regions considered in the present work – West NEU, East NEU, West CEU, East CEU, West SEU, East SEU. (Outliers are not shown).

of events of different types. In the present case, we consider Precipitation (P) and Soil Moisture (SM) events. It is a particularly useful tool in climatic studies (He and Sheffield, 2020; Manoj et al., 2022; Sun et al., 2018, 2017) and helps to consider the timings of certain well-defined

events. It has found varied applications in earth sciences and allied fields. Some of the more recent works include – exploring the global transition between droughts and pluvial events (drought – pluvial seesaw) (He and Sheffield, 2020), constructing a functional network

from gridded precipitation data to study the changes in spatiotemporal patterns of monsoons over East Asia (Wolf et al., 2021), deriving statistical relationships between El Nino Southern Oscillation (ENSO) episodes and drought occurrence over China (Xing et al., 2022) and evaluating the occurrence of flooding preceded by heat stress over Central United States (Zhang and Villarini, 2020). However, none of the previous studies have included simultaneously soil moisture, precipitation, and flood discharge data to contextualise the relative importance of SM-P coincidence as a peak flood discharge mechanism.

The first step in the analysis involves setting the hypothesis that events in SM precede events in P. In our case of quantifying SM-P coincidence, this ensures that SM events occur before P events. Hence, the trivial case of SM arising well after P has already occurred is not counted as a coincidence. ECA affords two parameters – the temporal tolerance window, ΔT and lag parameter τ and counts the mutual occurrences of events P and SM within the temporal tolerance interval ΔT . To characterise the probability of SM preceding P, ECA provides the precursor coincidence rate (r_p).

The main purpose of the precursor coincidence rate is to identify (out of the total P events) those events preceded by at least one SM event in the preselected temporal window. The resulting number of SM-P coincidences is reported as a fraction of the total number of P events. Consider event series of type P and SM in which the events occur at times t_i^P and t_j^{SM} with $i = 1, \dots, N_P$ and $j = 1, \dots, N_{SM}$, where N_P and N_{SM} are the total numbers of events in series P and SM, respectively. The precursor coincidence rate (r_p) is defined as (Donges et al., 2016, 2011)

$$r_p = \frac{1}{N_P} \sum_{i=1}^{N_P} H \left(\sum_{j=1}^{N_{SM}} I_{[0, \Delta T]} \left((t_i^P - \tau) - t_j^{SM} \right) \right) \quad (1)$$

where τ is the lag parameter, ΔT is the temporal tolerance. $I_{[0, \Delta T]}(\cdot)$ is the indicator function defined as:

$$I_{[0, \Delta T]}(x) = \begin{cases} 1, & x \in [0, \Delta T] \\ 0, & \text{else} \end{cases} \quad (2)$$

The Heaviside function is further expressed as:

$$H(x) = \begin{cases} 1, & x > 0 \\ 0, & \text{else} \end{cases} \quad (3)$$

r_p measures the fraction of P-type events preceded by at least one - SM type event. It can range from 0 to 1. Zero indicates the complete absence of any coincidence, and one denotes that all events in series P happen coincident with events in SM. Attention is invited to the fact that multiple coincidences with the temporal window ΔT is only counted once.

The 95th percentile limit defined the P and SM events at each grid point (Detailed information provided in Data Preparation, Section – 3.1). Temporal tolerance (ΔT) was selected as three days. The lag parameter τ , which can allow for the shifting of events, is not considered in our analysis and is set as 0 hereafter. A sensitivity analysis previously conducted by changing the temporal tolerance (ΔT) windows to five days and seven days showed that the spatial patterns remain relatively consistent for the different windows and hence considering the resolution of the grid, the data and the spatial extension of the study area, we only discuss the results for three days throughout the remainder of the paper.

The obtained coincidence rates at each grid point are tested with the Poisson distribution for statistical significance to assess the robustness. (Donges et al., 2016; Xing et al., 2022). The null hypothesis is set as the observed coincidence values being explained by two randomly generated event series following the Poisson distribution. The p-value of the significance test gives the probability that the actual observed number of coincidences is equalled or exceeded in the randomly generated samples. If the p-value is less than the selected confidence level α (0.05), the null hypothesis is summarily rejected, and the coincidence rate obtained is considered significant enough (Manoj et al., 2022). Detailed

information regarding the significance test is given in [Supplementary Information](#). Statistically insignificant values are not considered and masked using NA in the main plots. ECA was implemented in R Statistical Computing Language (v4.0.2: [r Core Team, 2021](#)) using the CoinCalc package (Siegmund et al., 2017).

3.3. Conditional event coincidence analysis (CECA)

Conditional Event Coincidence Analysis is an extension of the basic bivariate ECA method, first introduced by Siegmund et al. (2016a); CECA advances the two-variable ECA approach to account for the conditioning of events on another third variable. More specifically, in addition to counting the coincidence between event series SM and P, we explore the instances in which a Q event (defined here as an annual peak discharge event) also appears coincident with the already evaluated SM-P coincidences. To characterise the probability of both SM and P preceding Q, CECA provide the conditional precursor coincidence rate (r_p^c).

The conditional precursor coincidence rate, r_p^c is defined as (Siegmund et al., 2016a):

$$r_p^c = \frac{1}{N_Q} \sum_{i=1}^{N_Q} H \left(\sum_{j=1}^{N_P} H \left[\sum_{k=1}^{N_{SM}} I_{[0, \Delta T_{cond}]} \left((t_j^P - \tau_{cond}) - t_k^{SM} \right) \right] I_{[0, \Delta T]} \left((t_i^Q - \tau) - t_j^P \right) \right) \quad (4)$$

t_i^Q , t_j^P , t_k^{SM} denote the timings and. N_P , N_{SM} and N_Q are the total numbers of events in series Q, P and SM, respectively. τ_{cond} and ΔT_{cond} are defined as the temporal lag and time window for checking the conditioning of events. We aim to identify (out of the total Type Q events) those Q events preceded by at least one joint SM-P episode in the pre-selected temporal window. The temporal tolerance windows (ΔT , ΔT_{cond}) are set as two and one day, respectively. A preliminary review of some of the previous flood events (in which antecedent conditions were reported to have played a significant role on flood initiation) showed that such a setting could account for most of such events (Blöschl et al., 2007; Dietze et al., 2022; Schröter et al., 2015).

r_p^c measures the fraction of Q-type events preceded by at least one SM conditioned P event. Intrinsically, only those events in P are checked for coincidence with Q, which are already conditioned by SM events. The possible range again varies from 0 to 1, with one denoting that all the discharge (Q) events occurred after SM-P episodes and 0 indicating the absence of any statistical coincidence relationship between Q and SM-P.

A detailed methodology diagram outlining the major steps involved in the analysis is shown in [Fig. 4](#). Furthermore, an explanation on the procedure for calculating the precursor and conditional precursor coincidence rates (r_p & r_p^c) is provided in Appendix – A in [Supplementary Information](#) using a prototypical example.

4. Results

In the present section, we first (4.1) explore the seasonal patterns of SM-P dependence over the major European climatic regions using the precursor coincidence rate; we then characterise the conditional precursor coincidence rate for discharge events appearing coincident with joint SM-P episodes (4.2).

4.1. Spatiotemporal patterns of SM-P coincidence

In winter (DJF), grid points with higher SM-P coincidence rates ($r_p > 0.50$), are seen in Southern Europe (SEU) and towards the western parts of Northern and Central Europe (NEU & CEU). Only sparse coincidence is reported in other regions of NEU and CEU. Except for the gradual reduction in magnitude and extent, similar patterns are seen for

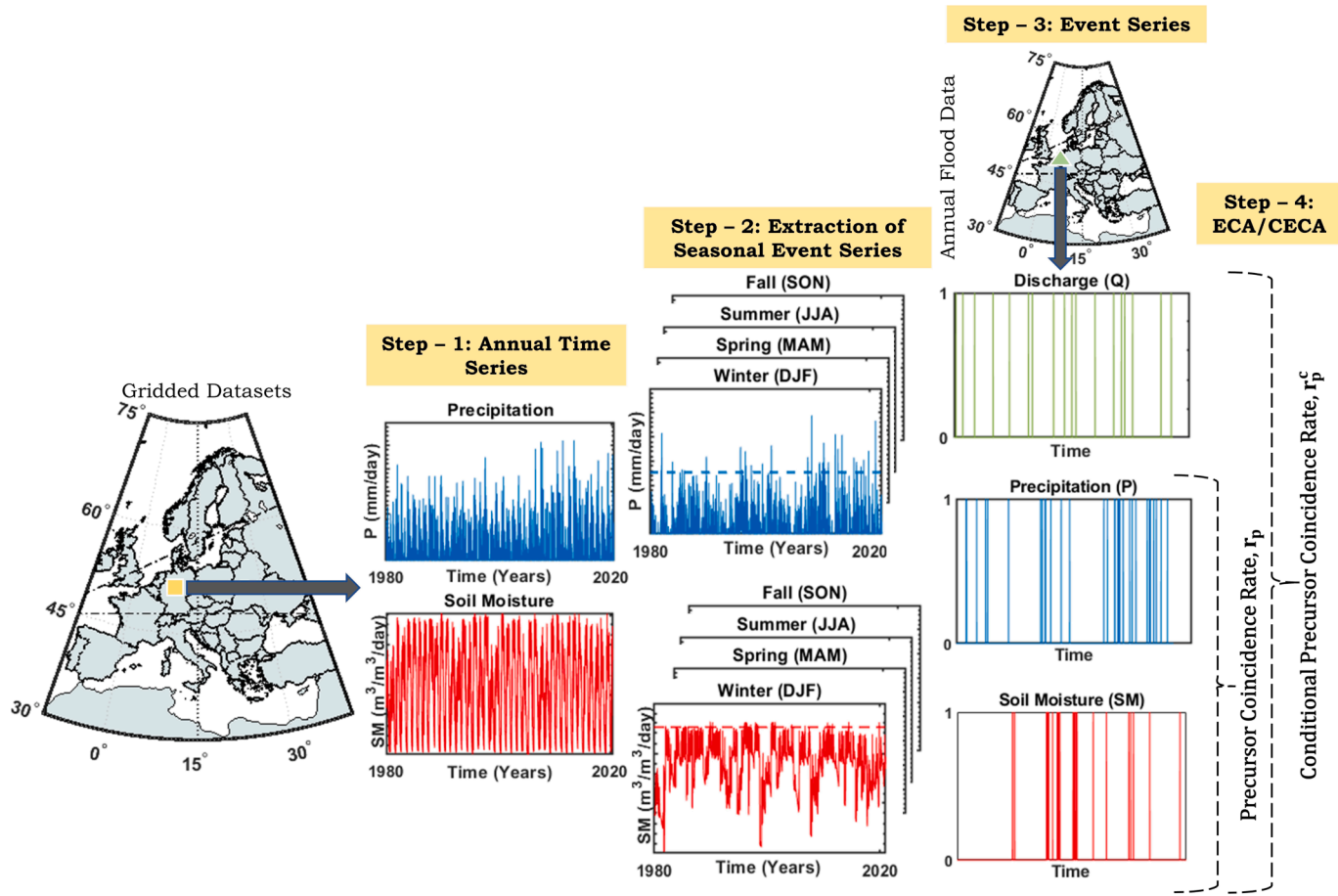


Fig. 4. Illustration showing the major steps involved in the analysis. Step – 1 represents the extraction of Precipitation (Blue) and Soil Moisture (Red) time series for a representative grid point. The annual time series is then split into seasonal timescales (DJF, MAM, JJA & SON). This is followed by applying the percentile cutoff to extract the seasonal event series (Step – 2). The dates of annual flood events are used to prepare the seasonal discharge event series (Green) in Step – 3. Also shown are the final binary event series for Precipitation (Blue) and Soil Moisture (Red). The event-based ECA analysis is carried out finally in Step – 4. First, we calculate the precursor coincidence rates (Section – 3.2) for P events preceded by an SM event. Then we calculate the conditional precursor coincidence rate (Section – 3.3) for discharge events happening after SM-P joint episodes that have already taken place. (For interpretation of the references to colour in this figure legend, the reader is referred to the web version of this article.)

the three major climatic regions in Spring (MAM). A seasonal shift in the location of high-valued clusters of precursor coincidence rate ($r_p > 0.50$) is seen in Summer (JJA). Higher coincidence now emerges in East CEU and NEU. A reduction in coincidence is seen for SEU. For Fall (SON), the coincidence rates reduce in NEU and CEU, and a gradual formation is seen again in SEU. From Fig. 5, it is clear that there is a strong seasonal nature to the coincidence rates over the major European climatic regions.

The spatial map plots help us understand and visualise the seasonal changes in precursor coincidence (r_p between SM and P for Europe). In general, the regions exhibit distinct seasonal behaviour. Apart from understanding the mean behaviour of the areas it also becomes essential to account for the distributions of r_p exhibited by them.

This apparent seasonality in the distribution of coincidence rates for grid points within the six regions is explored further using a violin plot in Fig. 6. Violin plots are an extension to the boxplots, showing the entire distribution of data at different values. It helps to check for multiple peaks in the probability density function and their relative position in the dataset. In the present case, the plots show the distribution of precursor coincidence rates among the grid points for the different regions. (Refer to Fig. 1 for the location of grid points and the explanation of the colour scheme used). Tails point to the presence of grid points with markedly different values of r_p compared to the median (mean) behaviour of the region.

Fig. 6 shows the violin plot for the six regions (West NEU, East NEU, West CEU, East CEU, West SEU, East SEU). Both the West and East SEU exhibit consistent behaviour in Winter. This contrasts with NEU and CEU, where higher median (mean) coincidence is seen towards the west compared to the eastern regions. For Spring, a slight increase in median (mean) coincidence is seen for both East CEU and SEU. From Fig. 6(C), it is also clear that the SM-P coincidence increases towards the East in Summer. The eastern regions exhibit higher median (mean) coincidence in the three regions compared to the western regions.

The seasonal patterns in the distribution of coincidence rates can be interpreted using the climatology of the three regions. Figs. 2 and 3 depict the monthly changes in mean daily values for precipitation and soil moisture for the six regions. The boxplots show how the average state of precipitation and soil moisture differs for the regions. Around May, the soil moisture starts declining considerably throughout the six climatic regions. In summer (JJA), the reduction in soil moisture is experienced throughout Europe. However, precipitation trends differ for SEU compared to NEU and CEU (Iturbide et al., 2020). Contrastingly, the precipitation reduces for both West and East SEU, while it shows an increasing trend for the regions in NEU and SEU.

Radiation and soil moisture availability have been consistently put forth as the two main drivers of evapotranspiration (ET) over Europe (Ghajarnia et al., 2020; Harris et al., 2017; Teuling et al., 2009). SEU's evapotranspiration (ET) regime is expected to be water-limited in nature

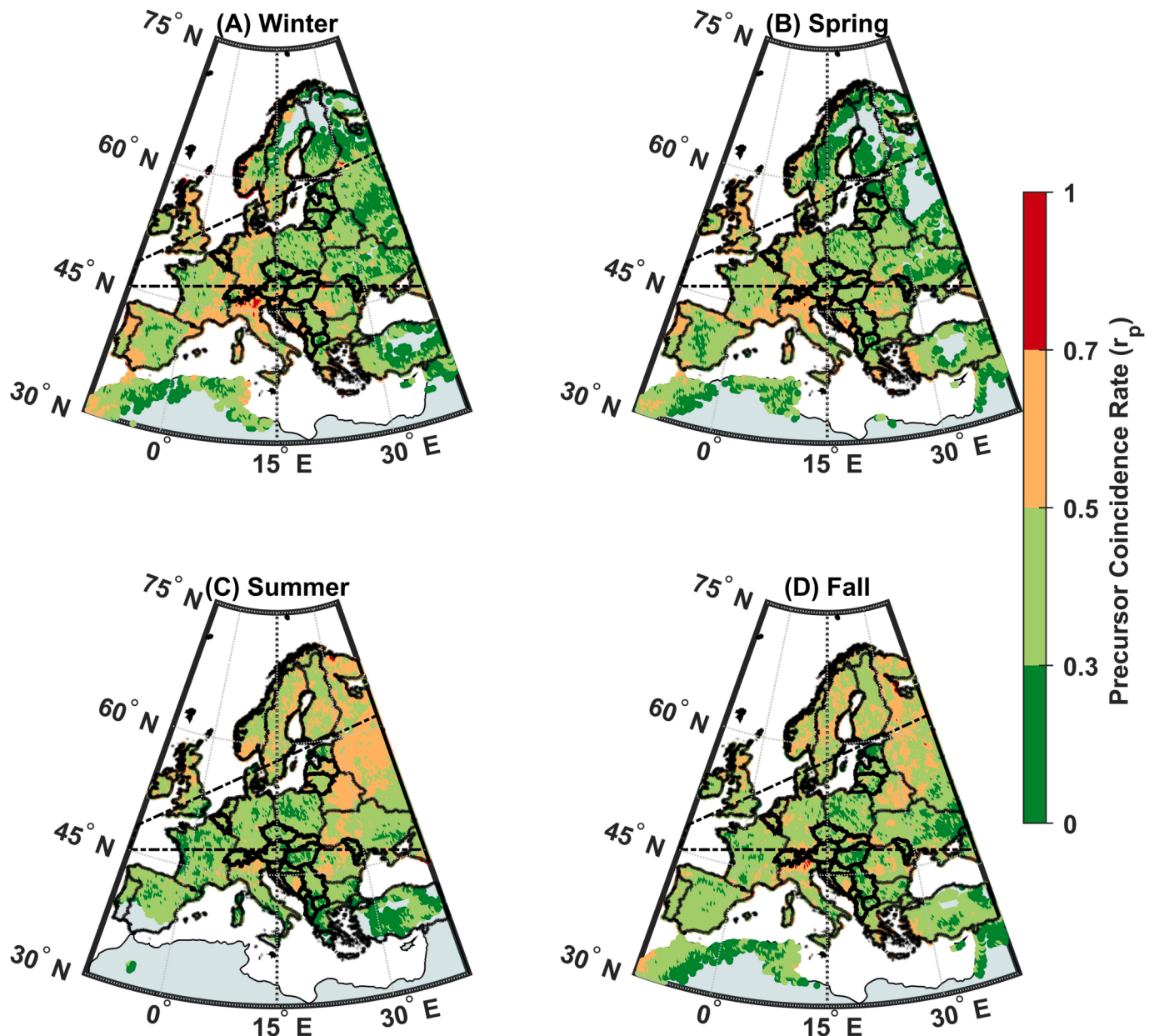


Fig. 5. The spatial patterns of SM-P coincidences from 1980 to 2020 characterised using the precursor coincidence rate (defined as the fraction of P events that are preceded by at least one SM event in the preselected temporal window) for different seasons – (A) – Winter (DJF), (B) – Spring (MAM), (C) – Summer (JJA) and (D) – Fall (SON). Colorbar denotes the precursor coincidence rate, r_p . Green denotes regions with precursor coincidence rates less than 0.50, and orange denotes areas with coincidence fractions between 0.50 and 0.70. Red denotes parts having coincidence greater than 0.70. (For interpretation of the references to colour in this figure legend, the reader is referred to the web version of this article.)

(Ghajarnia et al., 2020). Thus, we expect less SM-P coupling via ET in SEU in the summer. This is seen in Figs. 5 and 6; Regions in SEU exhibit only moderate coincidence in summer and have the lowest median (mean) value. The precipitation in SEU starts to increase around mid-Fall, which increases soil moisture. This leads to an increase in ET, which may be one of the reasons for the rise in coincidence seen for SEU in Winter (DJF). For both NEU and CEU, the ET regime is expected to be primarily energy-limited (Ghajarnia et al., 2020), and hence we see stronger coincidence and higher median (mean) values in Summer when the temperature (energy supply for ET) is also high and provides a conducive environment for enhanced SM-P coupling. The dependence of ET trends on radiation trends in central Europe was also suggested by (Teuling et al., 2009). However, it should be noted that further analysis incorporating ET and radiation input should be carried out to verify the proposed role of ET in impacting the SM-P coincidence rates. Previous

studies have assessed the impact of land cover and temperature changes for the seasonal evolution of evapotranspiration and related water cycle changes over Europe (Hänsel et al., 2019; Nistor et al., 2018). This presents a very interesting avenue worth exploring in future studies.

The difference in patterns seen for the East NEU and East CEU can partly be explained by the extensive snow cover usually found in those regions during Winter and Spring (Berghuijs et al., 2019b; Kemter et al., 2020). In Summer, we see a corresponding rise due to snow melt and a shift of snowfall to rainfall when air temperatures start rising above zero (Di Sante et al., 2021; Hundecha et al., 2020) in SM-P coincidence values. The near-identical behaviour manifested in West and East SEU throughout the different seasons can be attributed to the typical Mediterranean climate of the regions (Mediero et al., 2015; Schär et al., 1999).

In addition to exposing the seasonal SM-P covariation patterns, it is

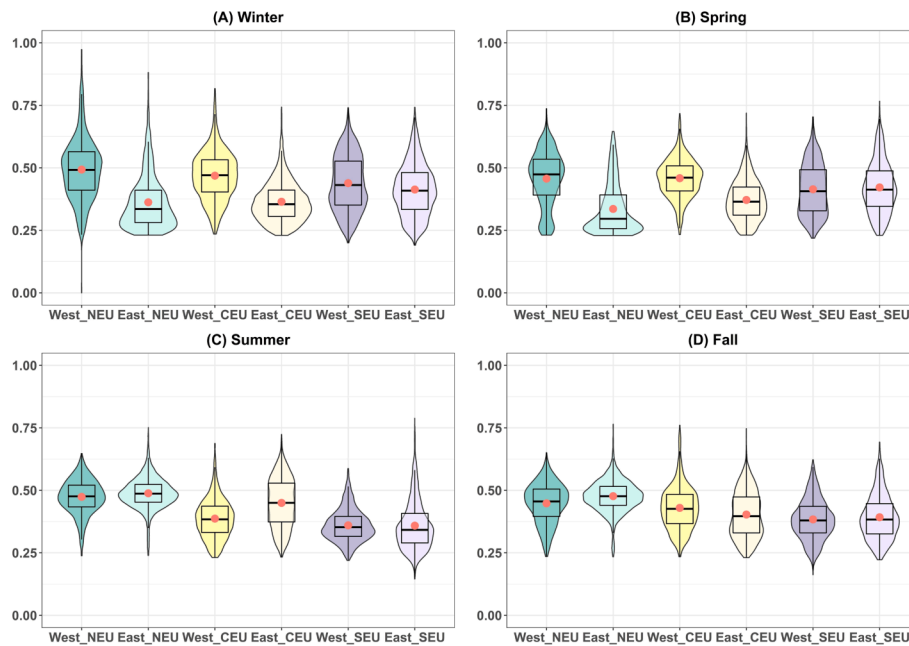


Fig. 6. Violin plots showing the seasonal shifts in the distribution of precursor coincidence rates among the grid points for the six regions. Red filled circle in the plot denotes the mean of the distribution. (For interpretation of the references to colour in this figure legend, the reader is referred to the web version of this article.)

also essential to know the role played by the SM-P dependence as a possible flood generation mechanism. This is attempted by contextualising the statistical precursor relationship between SM-P coincidences and the dates of occurrence of annual peak floods over European catchments using the conditional precursor coincidence rate (r_p^c).

4.2. Seasonal SM-P coincidence prior to annual peak floods

To understand the possible role of SM-P coincidences unravelled in 4.1 as a candidate mechanism for flood-generation over Europe, we used the European Flood Database (Hall et al., 2015) consisting of dates of occurrences of annual peak floods. More specifically, we consider the coincidence of the discharge events (Q) with precipitation events (P) that occurred on soil moisture anomalous states (SM). The conditional precursor coincidence rate (r_p^c) of a catchment in a particular season is the fraction of annual floods (out of the total number of reported floods in that season) happening after the joint occurrence of both SM & P events. The setting helps to account for the fraction of annual flood events in a particular season that occurred after precipitation extremes happened in saturated soil conditions.

In this work, we focus our analysis on the statistically significant results. Additionally, as complementary information, the analysis considering all coincidence rates (both significant and non-significant) is included in Figs. C3-C5 in Appendix C (Supplementary Information).

Fig. 7 depicts the seasonal patterns for the conditional precursor coincidence of Q with SM-P coincidence over European catchments. The physical interpretation of the conditional precursor coincidence rates (r_p^c) is the fraction of annual floods in a particular catchment after SM-P preconditioning. We hypothesise that soil moisture excess runoff is one of the driving mechanisms for flood generation in catchments with higher conditional precursor coincidence rates. These are the catchments where a higher fraction of annual floods happened in wet conditions (based on the exceedance above the 95th percentile limit). The role played by the catchment wetness in shaping the runoff response in these catchment areas can be considered more critical than the catchments with lower conditional precursor coincidence rates.

Higher coincidence rates ($r_p^c > 0.70$) are reported for SEU and in the

western European countries (Germany, Belgium, France, and UK) in winter. This contrasts with the sparse coincidence rates in Scandinavian and Eastern European catchments. For Spring, a clear east to west continental divide is seen in the spatial distribution of the conditional precursor coincidence rates. Higher coincidences are seen towards the west of 15° longitude and lower coincidence to the east. We also note the gradual emergence of significant coincidence rates in catchments towards Scandinavia and Eastern Europe, which were absent in winter. However, the rates are still lower ($r_p^c < 0.50$) compared to western catchments. For summer, clusters are seen in CEU, particularly in the Alps and the Carpathian Mountain ranges. Only nominal coincidence rates are seen in SEU. For Fall, we see strong coincidence rates ($r_p^c > 0.70$) for the UK, parts of Norway and Alpine regions.

Next, we focus our attention on the mean seasonal behaviour of the conditional coincidence rate among all the catchments in our study area. To investigate the changes in conditional precursor coincidence rates seasonally throughout Europe, we plotted seasonal violin distribution plots considering all the catchments with a significant coincidence rate.

Fig. 8 shows an average increase in the median (mean) coincidence from winter to fall for these catchments. A comparison between winter and Spring shows that, even though the median (mean) and the number of samples are very similar for both seasons, the coincidence rates among the catchments are slightly more spread out in Spring. The median coincidence is highest in Fall (0.67), which indicates that at least half of the catchments in Fall have two-thirds or more of the annual floods occurring shortly after the joint occurrence of high antecedent soil moisture conditions and precipitation events.

Similar to the regional distribution plot of the SM-P precursor coincidence rate, we also plotted violin box plots of the seasonal conditional coincidence rate distributions among the catchments for the six sub-regions (Fig. 9). We see noticeable changes in the distribution of the coincidence rates for catchments in the six regions, in line with the expected flood seasonality and evolution of SM-P coincidence described earlier.

For winter, the emergence of high valued conditional coincidence rates (r_p^c) in catchments over SEU corresponds to the increased SM-P coincidence rates reported for the region (r_p) in Fig. 3. In summer, similar to the reduction of mean SM-P coincidence, we see very sparse

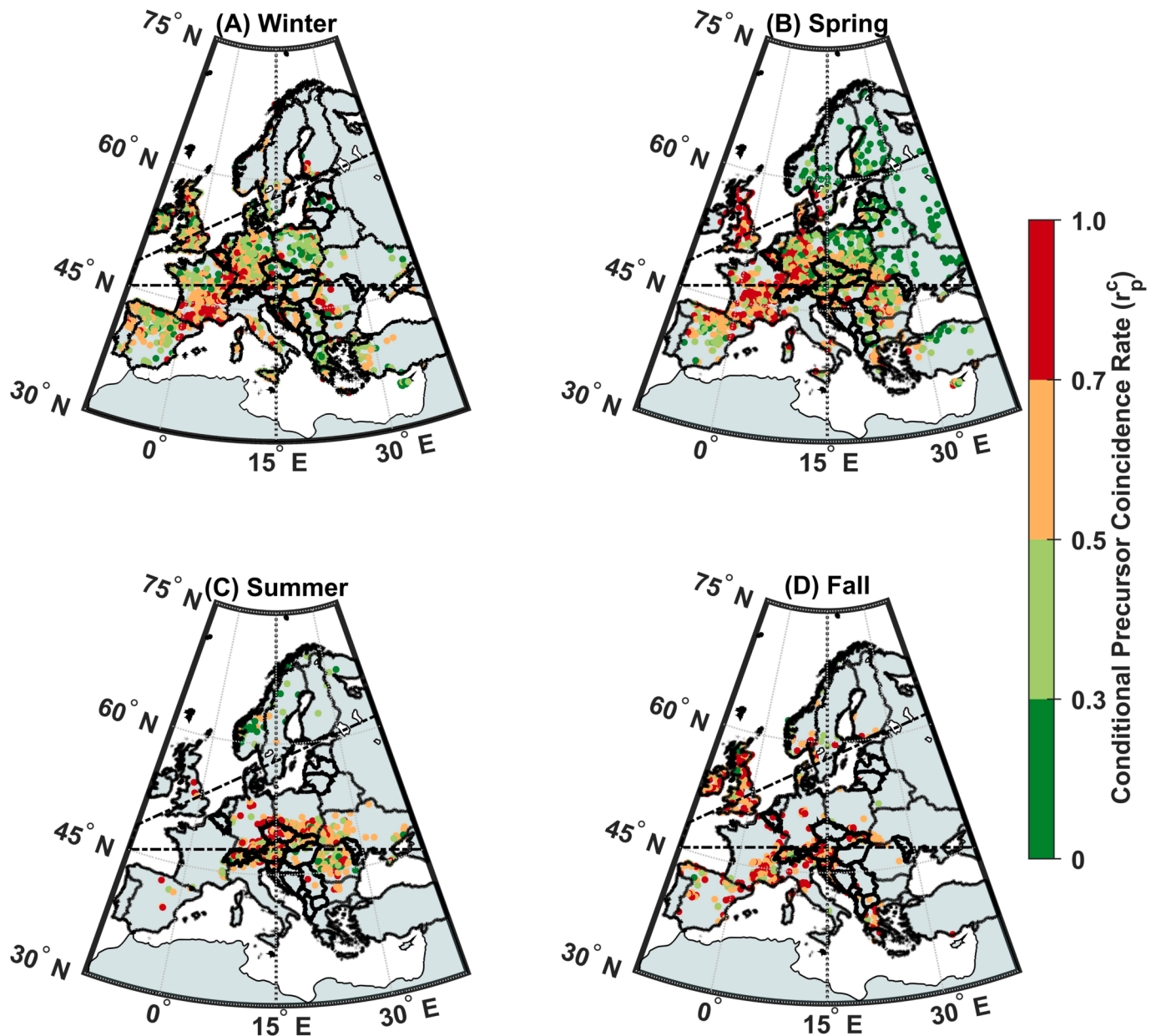


Fig. 7. The seasonal variation in conditional precursor coincidence rates (defined as the fraction of discharge events that are preceded by the joint occurrence of both P and SM events within the selected tolerance window) for catchments over Europe from 1980 to 2010. Figure (A) denotes precursor coincidence for Winter – DJF, Figure (B) for Spring – MAM, Figure (C) for Summer – JJA and Figure (D) for Fall – SON. Green denotes regions with conditional precursor coincidence rates less than 0.50, and orange denotes areas with coincidence fractions between 0.50 and 0.70. Red denotes parts having coincidence greater than 0.70. (For interpretation of the references to colour in this figure legend, the reader is referred to the web version of this article.)

conditional coincidence rates for the catchments. The conditional precursor coincidence rates (r_p^c) again gradually emerge in Fall over SEU, which coincides with the increase in median (mean) SM-P coincidences (r_p). This is interesting as even though higher rates of precursor coincidence mean more SM-P joint episodes, a higher r_p value might not always directly translate into a higher r_p^c value, as the conditional precursor coincidence is characterised by the total number of Q events whereas the precursor coincidence is reported as a fraction of the total number of P events.

The higher conditional coincidence rates towards the countries of Western Europe indicate the importance of soil moisture excess in driving floods in Winter and Spring. Previous studies found that persistent precipitation events due to westerly winds from the Atlantic is a major factor in the generation of floods over the region (Ibebuchi, 2022; Lun et al., 2021; Mediero et al., 2015; Zanardo et al., 2019). Such

persistent precipitation episodes can lead to increased catchment wetness and, subsequently higher conditional coincidence.

The absence of significant coincidence rates for catchments towards eastern Europe and Scandinavia in Winter can be ascribed to the low winter temperatures preventing snowmelt and leading to snow accumulation. Significant coincidence rates gradually emerge in Spring; however, the lower values indicate the relative less importance of SM-P coincidence as a peak flood generation mechanism in the region. For the Alpine region, the higher conditional coincidence rates in Summer may be due to the role played by summer rainfall and snowmelt. Snowmelt usually starts in spring and saturates the soil for the summer rainfall events. In the presence of melting snow, soils will get saturated leading to higher conditional coincidence rates for the flood events with P and SM events. However, it should also be noted that snow accumulation and melting processes depend on the mean elevation of the catchment

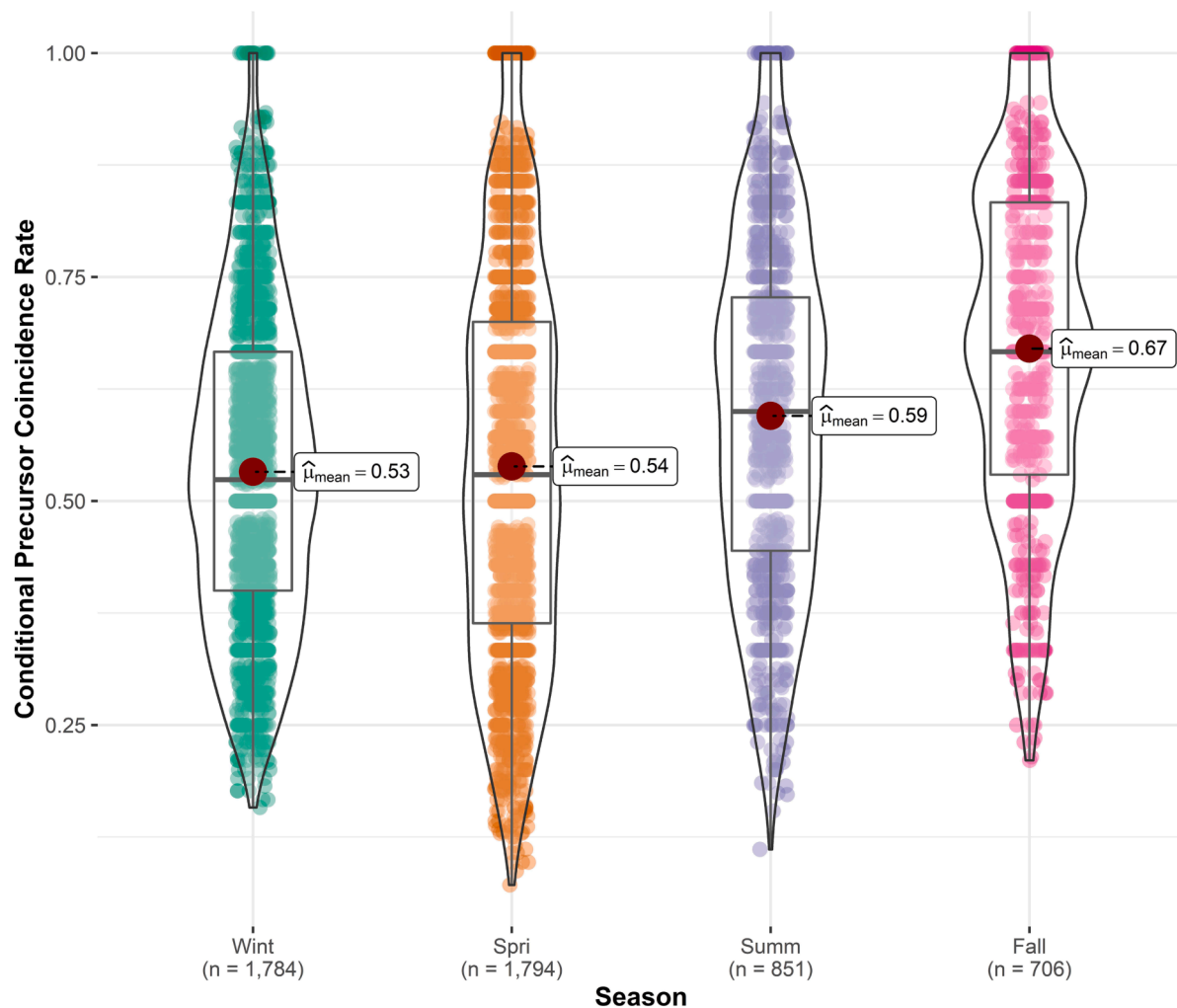


Fig. 8. Violin plot with an included boxplot showing the distribution of conditional precursor coincidence rate (defined as the fraction of discharge events preceded by the joint occurrence of both P and SM events within the selected tolerance window) seasonally for catchments over Europe. Red pointer indicates the mean of the distribution. The number of catchments considered is also shown below the respective seasonal plots. (For interpretation of the references to colour in this figure legend, the reader is referred to the web version of this article.)

above sea level, which could impact the coincidence rates.

5. Discussions

The current study made use of event based ECA approach to describe the spatiotemporal patterns of SM-P dependence over Europe and then visualised the changing seasonal nature of such SM-P covariation patterns over the different climatic regions. The SM-P coincidence was characterised by the precursor coincidence rates. We then investigated the relative importance of SM-P coincidence as a possible precursor to the annual flood events using the conditional precursor coincidence rate.

5.1. Understanding the seasonal SM-P coincidence patterns

The fact that the joint manifestation of P events and SM anomalous conditions within a short interval can lead to highly nonlinear catchment response and hazard cascades is already well noted in the literature (Berghuijs et al., 2019b; Brocca et al., 2012; Ray and Jacobs, 2007; Wasko et al., 2020). It is worth mentioning here that SM anomalies are not only caused by extreme precipitation, but even sustained sub-extreme precipitation can manifest into soil moisture anomalies. These antecedent conditions contribute to flood generation only during any subsequent rainfall events, and the SM-P coincidence analysis helps to

understand and account for them. Univariate modelling approaches, which only focus on the precipitation characteristics, severely under-represent such nonlinear catchment feedback mechanisms. Previous studies were also constrained by the direct trivial relationship arising between precipitation and soil moisture (Seneviratne et al., 2010). Due to its directional formulation, ECA allows quantifying such dynamic feedback between SM and P.

The SM-P coincidence analysis gives potential insights into the covariation relationship between soil moisture and precipitation at a particular grid point. Essentially, it denotes the fraction of P events, which occurred after SM also exceeded its threshold. It can also be related to the conditional/joint probability that both variables attained their exceedance conditions together. The temporal tolerance window helps to also account for dynamical interdependencies that cannot be easily captured by linear correlation/covariation measures.

Floods usually occur due to a complex interplay between atmospheric processes and factors contributing to runoff generation in the catchment (Merz et al., 2021). The coincidence rates are also defined by both geomorphological and climatic factors.

One possible explanation for higher conditional rates is that extreme precipitation events in the region are usually preceded by a period of sustained duration precipitation. The higher coincidence values could be an indicator of the persistence of soil moisture memory in a particular region. The soils in these regions can store information on previous

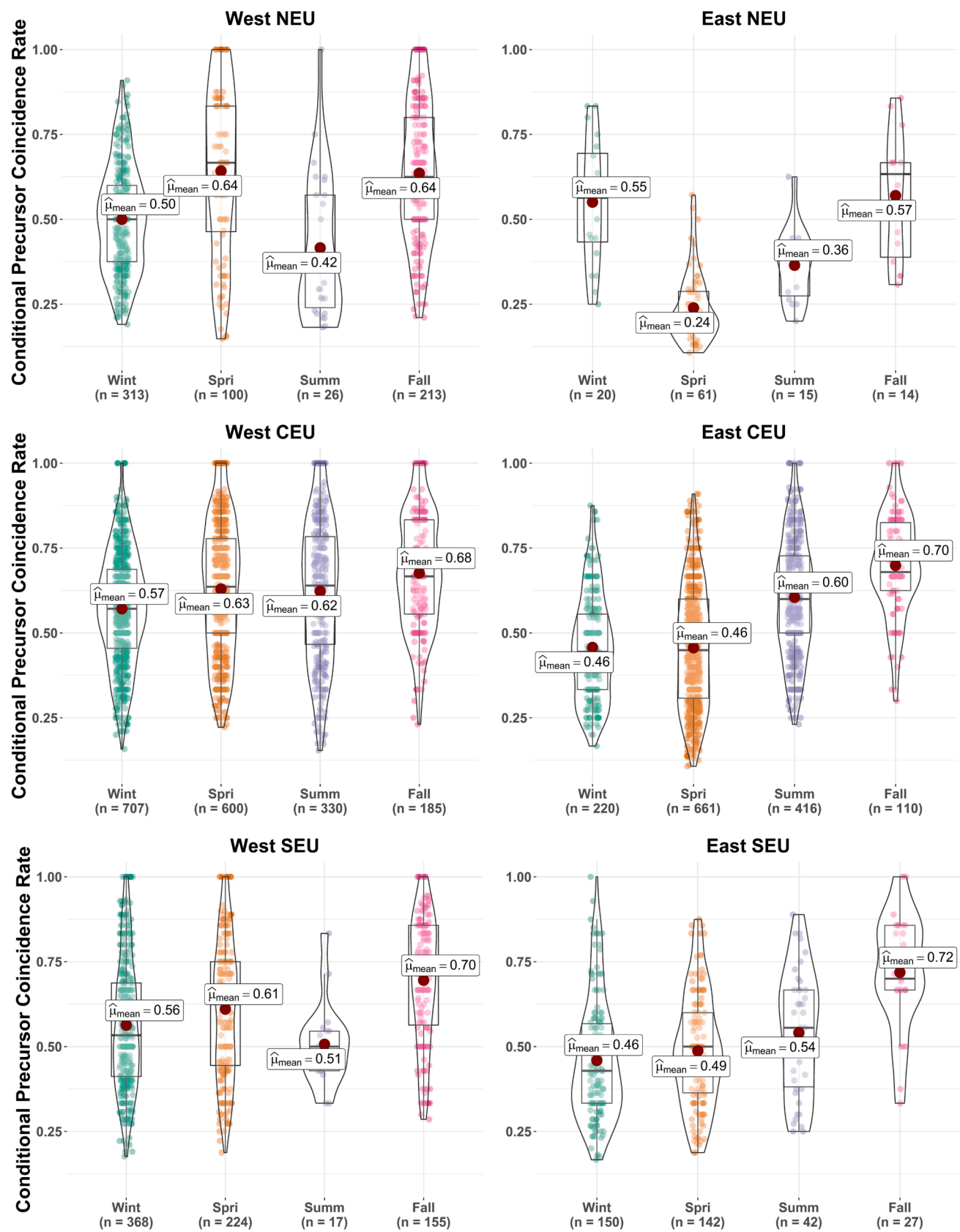


Fig. 9. Regional distribution plots showing the seasonal evolution of conditional precursor coincidence rates.

precipitation events for a more extended period. This could be related to soil properties, including soil type, texture, the land use and land cover of the region. Another factor could be the triggering relationship between soil moisture and precipitation (Brimelow et al., 2011; Manoj et al., 2022; Schwingshackl et al., 2017; Seneviratne et al., 2010) via direct (evapotranspiration) and indirect interactions (non-linear impacts on boundary layer stability, convective precipitation formation). The SM-P coincidence analysis suggests that seasonality is a major process in the spatiotemporal dynamics of SM-P covariability over Europe. Previous works have tried to unravel such dynamic spatial patterns at a continental scale for Europe mainly from a perspective of dry conditions, i.e., droughts (Bonaccorso et al., 2013; Hannaford et al., 2011; Tallaksen and Stahl, 2014). We argue that our analysis provides valuable information on spatial patterns of hydroclimatic covariability with a focus on wet conditions. Our results also show the need for considering spatial heterogeneity within the three IPCC homogeneous regions. Studies which use such homogeneous regions as references for the regional synthesis of future climate projections (Iturbide et al., 2020) should take care of the varying nature of seasonal SM-P coupling behaviour within the reference regions. Attributing the cause of such coupled SM-P relationship would require process-based models for the regions, in which different scenarios should be investigated to test different hypothesis. Such an analysis is worth investigating but goes beyond the capabilities of the methodology applied in this work which is based solely on the statistical properties of the considered datasets.

5.2. SM-P dependence characteristics of the different climatic regions

Spatially well-defined clusters are seen in southern Europe (SEU), West NEU and West CEU in Winter, which shifts towards eastern Europe in summer. Our results are generally in agreement with previous SM-P studies over Europe. The reduction in soil moisture, precipitation, and evapotranspiration for SEU in summer was shown by Ghajarnia et al. (2020) using a data-driven multi-catchment approach. They observed higher monthly correlation values between soil moisture and evapotranspiration in the summer for SEU. Their work stressed the critical role played by soil moisture in regulating large-scale runoff variations across diverse European climatic regions.

The violin plots further helped understand the distribution of SM-P coincidence rates within major IPCC regions over Europe and their seasonality. The reduction in median (mean) coincidence rates among grid points in SEU is well captured in the seasonal violin plots. Such a reduction in coincidences is likely due to drier soil moisture states and less SM-P coupling via ET during summer in SEU. The resulting plots further pointed to the spatial variation of SM-P coincidence rates within NEU and CEU. The near identical distribution of precursor coincidence rates for both West and East SEU is an indicator of the homogenous behaviour of the whole region (SEU) w.r.t hydroclimatic coupling.

Identifying such homogenous regions and their corresponding seasonal behaviour is crucial for numerous hydro-meteorological applications (Agarwal et al., 2018; Guntu et al., 2020; Pérez Ciria and Chiogna, 2020). They can aid in disentangling the complexity of hydrological systems (McDonnell and Woods, 2004). The spatial coherence of such changing regional patterns can hold vital information about the propagation of large-scale hydro-meteorological extremes like droughts and floods.

The role of soil moisture-atmosphere coupling for temperature and precipitation extremes and their associated trends have also been previously studied over Europe. Jaeger and Seneviratne (2011) used simulations from a regional climate model to investigate the role of SM-P coupling for temperature and precipitation extremes over the European summer climate. Significant impacts of temporal SM variability were found for the wet-day frequency and other associated extreme indices. Seneviratne et al. (2006) investigated the role of atmospheric coupling on future changes in the interannual variability of summer precipitation over Europe and found that, in most cases, the deviations can be partly

explained by land-atmosphere coupling. In regions where precipitation increases of considerable magnitude were simulated, the land-atmosphere coupling could account for about two-thirds of the total variance.

5.3. SM-P dependence as a possible flood generation mechanism

Accounting for the impact of joint SM-P covariation patterns in the context of annual flood generation over European catchments is vital for the proper characterisation of different possible runoff generation mechanisms. Identifying catchments with a higher fraction of reported historical annual floods immediately after the joint occurrence of SM-P coincidences and their dependence on seasonality is also helpful from flood forecast and disaster preparedness aspects. We used an extension of the bivariate Event Coincidence Analysis to account for the conditional probability of event occurrences in more than two variables. Specifically, we focused on discharge events (Q: Annual Floods) happening after both SM and P events have taken place.

Our findings showed that the seasonal evolution of such conditional precursor coincidence rates (r_p^c) over European catchments are generally in line with previous studies (Berghuijs et al., 2019b; Blöschl et al., 2019; Hundeicha et al., 2020; Lun et al., 2021). We saw an increase in the median (mean) coincidence for r_p^c from Winter to Fall, albeit with fewer catchments contributing to the distribution of the coincidence rates in Fall. Furthermore, we saw that the seasonal evolution of conditional precursor (r_p^c) over SEU is in line with the corresponding temporal changes seen in SM-P coincidence (r_p) patterns. To understand the possible connection between catchment wetness and the conditional precursor coincidence rates, we plotted the seasonal variation of the 95th percentile limit (Fig. C1 and C2 in Appendix – C, [Supplementary Information](#)). In general, we can observe higher values for soil moisture and precipitation limits in regions with higher coincidence rates.

Our observations align with the results of Berghuijs et al., (2019b) for Europe, who used seasonal statistics to estimate the relative importance of different mechanisms as potential flood drivers. They found that during 1960–2010 relatively few annual floods were caused by precipitation extremes acting alone, and in about 43% of the studied catchments, the flood events were caused by the concurrence of heavy precipitation with high antecedent soil moisture. The timing of soil moisture excess was seen to coincide with the seasonality of annual flood events across large parts of western Europe, including – Germany, France, Spain and Britain. These regions also have a higher coincidence in our case. The peak floods were also seen to not coincide in the case of eastern Europe. This behaviour is also seen in our analysis, with lower coincidence rates reported for the eastern European and Scandinavian catchments. However, caution should be given to the fact that the conditional coincidence rates are calculated out of the total number of events in a season.

Blöschl et al., (2019) demonstrated regional patterns in observed flood discharges over Europe and reported an increase in flood discharge values for north-western Europe – including parts of Germany, France and the Northern UK due to the increase in rainfall and soil moisture. Statistically significant positive correlation values were obtained for temporal variability of discharge and soil moisture maxima, which again points to the possible role played by soil moisture excess (along with the increasing precipitation) as an important flood driver for these regions. For southern Europe, a decrease in precipitation and soil moisture was reported, resulting in a decrease in flood discharge values from 1960 to 2010. The decline has been attributed to the northward shift of the subtropical jet and increased evapotranspiration due to warming temperatures (Archer and Caldeira, 2008; Mediero et al., 2014). We argue here that since the percentile thresholds (and the subsequent events) are calculated based on the long-term seasonal climatology of the region, such a reduction would lead to a fewer number of coincidences and, finally to a reduced coincidence rate. This could be a possible reason for lower rates seen in those regions. However, the characterisation of the

strength of absolute values on the calculated rates is indeed complex and worth investigating in detail in future studies.

Hundecha et al. (2020) identified four major flood-generating processes across Europe (long-rain, short-rain, snowmelt, and rain-on-dry-soil flood events) and investigated the seasonal and regional distribution of the different flood event types. They saw a clear predominance of short rain events (in which the catchment is saturated at the onset with very little soil moisture deficit) both seasonally and regionally throughout Europe. The only exception is the regions in Northern Europe where snowmelt events dominated. This is again similar to our observation of fewer significant conditional precursor coincidence rates in those regions, while at the same time, it should be noted that the coincidence rates is not generalised for all the other areas. Lun et al. (2021) did a pan-European assessment of characteristics and process controls of statistical flood moments. They used the mean annual flood (MAF) and coefficients of variation (CV) and skewness (CS) of flood discharges over five predetermined hydroclimatic regions. Similar to our results of higher conditional coincidence rates, they observed higher mean specific annual floods over regions of the Alps, the Apennines (Italy), the Carpathian Flysch Belt and Great Britain. The spatial patterns of CV showed that the consistency of the occurrence of such peak flows is also in line with our obtained results. Catchments with wetter states (In our case, higher conditional coincidence rates) showed less CV and hence more regularity in the occurrence of large floods.

5.4. Assumptions and limitations

The need for exercising caution while employing gridded products for the analysis of extremes at a daily scale is already well reported in the literature (Gervais et al., 2014; Timmermans et al., 2019). Since it is an observational dataset, the E-OBS product severely underperforms in regions with low station density, which can be considered one of the product's major limitations. However, we note here that since the initial release of E-OBS (Haylock et al., 2008), many more station has been continuously added and also the newer versions of E-OBS uses a refined interpolation method and take into account the possible uncertainties by delivering an ensemble of possible realisations (100 members) (Corney et al., 2018).

Moreover, in our case of quantifying the SM-P coincidence, we only consider the relative timings of events for different grid points. The ECA framework discards the magnitudes of the variable and only considers the days which exceed the prefixed percentile thresholds. Hence, we explored the time variability rather than absolute values of soil moisture; this has the advantage that, the choice of modelled product is expected to have a limited impact on the final calculated coincidence rates (Koster et al., 2009).

Our method is designed to quantify the SM-P dependence based on the mutual occurrence of events in both series within the prefixed temporal tolerance. We do not include the magnitude of such events into account. Therefore, a quantitative understanding of the possible impact of changes in the magnitude of precipitation on the SM-P dependence is lacking. The 95th percentile is a reasonable cut off to include all (extreme) precipitation events, which would finally lead to annual peak floods over the catchment. However, some floods could have been caused by rainfall rates not belonging to the top 5%, and our present analysis does not take into account such events.

The spatial resolution of the gridded data ($0.25^\circ \times 0.25^\circ$) provides an average representation of the precipitation characteristics occurring in a region. The grid-based soil moisture product is also averaged over considerable spatial heterogeneity. In order to compare the results for a larger number of catchments and to avoid the significant computational pre-processing work involved in carrying out a catchment area-weighted approach, we used the grid points of the catchment outlet. These approximations will invariably lead to a lack of representation of any small-scale site-specific conditions. However, our results must be seen as a first estimate of the catchments where significant dependence exists

between SM-P coincidences and the peak discharge events (in our case, higher conditional coincidence rates). Further works could focus on the identified locations and investigate the events following a process-based modelling approach. The methodology could be easily expanded to account for the catchment averaged soil moisture and precipitation values. The temporal tolerance window could also be adapted, and for a more detailed analysis, an approach involving the coincidence rates calculation for different temporal tolerance could be utilised.

We stress here that the hydrological processes leading to flood generation are nonlinear and difficult to characterise using only simple event-based approaches. Our main aim is to understand how the timing of the annual peak flood events could be used in conjunction with the seasonal patterns of SM-P dependence to get a first estimate of the locations experiencing annual floods shortly after SM-P coincidence. The relative ratio of such flood events in each season to the total number of flood events reported in the specific season is calculated and helps identify catchments that are more prone to such soil moisture excess-driven floods. Since only the dates of peak floods are available, it is again not possible to identify the changes in patterns for different magnitude events.

We caution that the absolute number of annual flood events reported in a season can vary for each catchment. The conditional precursor coincidence rates are reported as a fraction of the total number of events in a season (minimum five) for a catchment. A drawback of such an approach is that it leads to some catchments being present in specific seasons only, and to a different number of catchments in different seasons. However, in the present study our objective is to understand the relative importance of SM-P coincidence as a possible precursor to the annual flood events throughout all the catchments, and hence we investigated the relative proportions of the events as the conditional precursor coincidence rate (r_p^c).

Floods usually manifest due to several complex interconnected factors (Merz et al., 2021; Mishra et al., 2022). We focused on soil moisture and precipitation, but we believe the analysis of other important factors could contribute to better understanding the flood triggers. These additional variables include topography, soil type and properties, land cover change and even the impact of sea-surface temperature anomalies. Another point to be noted is the impact of anthropogenic constructions and the effect of reservoir management operations on streamflow alterations and variability (Pérez Ciriá et al., 2019).

6. Conclusions and perspectives

The present work provides a continental scale overview of the statistical coincidence relationship between soil moisture and precipitation events over Europe. We used the precursor coincidence rate to characterise the SM-P preconditioning and then investigated the influence of seasonality on the dependence strength. The changing patterns of SM-P dependence are studied in depth for the various climatic regions of Europe. The possible impact of such SM-P coincidences on annual flood events is also unravelled, focusing on the role of such antecedent conditions as a possible flood-generating mechanism.

The salient findings of the current study are:

- The seasonal SM-P coincidence analysis reveals that seasonality is a major driving force in the spatiotemporal dynamics of SM-P coupling over Europe.
- Higher coincidence rates are seen in Southern Europe (SEU) and towards the western parts of Northern and Central Europe (West NEU & West CEU) in Winter, which shifts towards East NEU and East CEU in Summer. The patterns are in line with the expected seasonal climatology of the different regions.
- The conditional precursor coincidence, which quantifies the relative fraction of annual flood events in a particular season that occurred after joint SM-P coincidence, is also evaluated for the different

catchments, and the observed values agree with previous flood hazard studies over Europe.

The present work can be advanced by conducting smaller catchment scale studies incorporating streamflow data. The relative impact of SM-P coincidence over a range of discharge values can also be investigated further. Exploiting the approach used in the present study to the problem of characterising the dependence of absolute values on the coincidence rates and the temporal evolution of the spatiotemporal patterns over the past few years provide an exciting avenue for future research but is beyond the scope of present study.

It is worthwhile to note that changing the temporal tolerance window parameters and studying their associated impacts could aid in understanding the lagged associations between the various hydrometeorological variables (In our case – soil moisture, precipitation, and discharge). Future works could investigate such lagged covariation relationships in detail by incorporating additional variables (for example, evapotranspiration, and solar radiation), evaluating the changes for different tolerance windows, and considering the lag parameters. Our results indicate the importance of considering antecedent conditions for understanding flood generation mechanisms over Europe. Event-based methods like ECA can help incorporate the conditioning of variables on other processes. ECA can be a vital tool in studies aiming to characterise multivariate dependencies. Approaches considering such dynamic relationships can vastly help describe multi-hazard risk scenarios and mitigate the adverse impacts of preconditioned compound events.

Data Availability Statement

We acknowledge the E-OBS (v24.0) dataset from the EU-FP6 project UERRA (<https://www.uerra.eu>) and the Copernicus Climate Change Service, and the data providers in the ECA&D project. The E-OBS product can be downloaded from the European Climate Assessment & Dataset website (<https://www.ecad.eu/download/ensembles/download.php>). The GLEAM product was accessed via the GLEAM homepage (<https://www.gleam.eu/>). The annual flood series are part of the European Flood Database and were downloaded from the Ingenieurhydrologie und Wassermengenwirtschaft website (<https://www.hydro.tuwien.ac.at/fileadmin/mediapool-hydro/Downloads/Data.zip>). The IPCC homogeneous regions shapefile can be retrieved from the GitHub ATLAS repository (<https://github.com/SantanderMetGroup/ATLAS>).

CRediT authorship contribution statement

Ashish Manoj J: Data curation, Formal analysis, Investigation, Methodology, Conceptualization, Resources, Software, Validation, Writing – original draft. **Teresa Pérez Ciria:** Investigation, Methodology, Conceptualization, Resources, Supervision, Writing – review & editing. **Gabriele Chiogna:** Funding acquisition, Conceptualization, Project administration, Supervision, Writing – review & editing. **Nadine Salzmänn:** Funding acquisition, Conceptualization, Supervision, Writing – review & editing. **Ankit Agarwal:** Funding acquisition, Conceptualization, Project administration, Supervision, Writing – review & editing.

Declaration of Competing Interest

The authors declare that they have no known competing financial interests or personal relationships that could have appeared to influence the work reported in this paper.

Data availability

Data will be made available on request.

Acknowledgements

AMJ acknowledges the financial support from MTech fellowship (Ministry of Education, Government of India at IIT Roorkee), DAAD KOSPIE Scholarship (German Academic Exchange Service, Funding ID-57588649) and ThinkSwiss Research Scholarship. TPC acknowledges the funding from the TUM ForTe – Forschungsförderung & Technologietransfer and from the EU Horizon 2020 innovation action programme ARSINOE (Climate-resilient regions through systemic solutions and innovations) under Grant Agreement 101037424. GC acknowledges funding from the DFG (Deutsche Forschungsgemeinschaft) Research Group (FOR2793/2) “Sensitivity of High Alpine Geosystems to Climate Change since 1850” (SEHAG) (Grant CH981/3-2). AA acknowledge the joint funding support from the University Grant Commission (UGC) and DAAD under the Indo-German Partnership in Higher Education (IGP) framework at the IIT Roorkee. AMJ would also like to thank Mr Ravi Kumar Guntu for helpful discussion and insights on Compound Events. The authors are grateful to the Editor and two anonymous reviewers for their helpful comments and suggestions which helped improve the overall readability and quality of the manuscript.

Appendix A. Supplementary data

Supplementary data to this article can be found online at <https://doi.org/10.1016/j.jhydrol.2023.129445>.

References

- Adamowski, K., Liang, G.C., Patry, G.G., 1998. Annual maxima and partial duration flood series analysis by parametric and non-parametric methods. *Hydrol. Process.* 12, 1685–1699. [https://doi.org/10.1002/\(SICI\)1099-1085\(199808/09\)12:10<1685::AID-HYP689>3.0.CO;2-7](https://doi.org/10.1002/(SICI)1099-1085(199808/09)12:10<1685::AID-HYP689>3.0.CO;2-7).
- Agarwal, A., Marwan, N., Maheswaran, R., Merz, B., Kurths, J., 2018. Quantifying the roles of single stations within homogeneous regions using complex network analysis. *J. Hydrol.* 563, 802–810. <https://doi.org/10.1016/j.jhydrol.2018.06.050>.
- Alfieri, L., Feyen, L., Dottori, F., Bianchi, A., 2015. Ensemble flood risk assessment in Europe under high end climate scenarios. *Glob. Environ. Chang.* 35, 199–212. <https://doi.org/10.1016/j.gloenvcha.2015.09.004>.
- Alsafadi, K., Al-Ansari, N., Mokhtar, A., Mohammed, S., Elbeltagi, A., Sh Sammen, S., Bi, S., 2022. An evapotranspiration deficit-based drought index to detect variability of terrestrial carbon productivity in the Middle East. *Environ. Res. Lett.* 17 <https://doi.org/10.1088/1748-9326/ac4765>.
- Archer, C.L., Caldeira, K., 2008. Historical trends in the jet streams. *Geophys. Res. Lett.* 35, L08803. <https://doi.org/10.1029/2008GL033614>.
- Bandhauer, M., Isotta, F., Lakatos, M., Lussana, C., Bäserud, L., Izsák, B., Szentes, O., Tveit, O.E., Frei, C., 2022. Evaluation of daily precipitation analyses in E-OBS (v19.0e) and ERA5 by comparison to regional high-resolution datasets in European regions. *Int. J. Climatol.* 42, 727–747. <https://doi.org/10.1002/joc.7269>.
- Barredo, J.I., 2007. Major flood disasters in Europe: 1950–2005. *Nat. Hazards* 42, 125–148. <https://doi.org/10.1007/s11069-006-9065-2>.
- Berghuijs, W.R., Allen, S.T., Harrigan, S., Kirchner, J.W., 2019a. Growing spatial scales of synchronous river flooding in Europe. *Geophys. Res. Lett.* 46, 1423–1428. <https://doi.org/10.1029/2018GL081883>.
- Berghuijs, W.R., Harrigan, S., Molnar, P., Slater, L.J., Kirchner, J.W., 2019b. The relative importance of different flood-generating mechanisms across Europe. *Water Resour. Res.* 55, 4582–4593. <https://doi.org/10.1029/2019WR024841>.
- Bertola, M., Viglione, A., Vorogushyn, S., Lun, D., Merz, B., Blöschl, G., 2021. Do small and large floods have the same drivers of change? A regional attribution analysis in Europe. *Hydrol. Earth Syst. Sci.* 25, 1347–1364. <https://doi.org/10.5194/hess-25-1347-2021>.
- Bevacqua, E., De Michele, C., Manning, C., Couasnon, A., Ribeiro, A.F.S., Ramos, A.M., Vignotto, E., Bastos, A., Blesić, S., Durante, F., Hillier, J., Oliveira, S.C., Pinto, J.G., Ragno, E., Rivoire, P., Saunders, K., van der Wiel, K., Wu, W., Zhang, T., Zscheischler, J., 2021. Guidelines for studying diverse types of compound weather and climate events. *Earth's Futur.* 9, 1–23. <https://doi.org/10.1029/2021EF002340>.
- Bezák, N., Brilly, M., Šraj, M., 2014. Comparison between the peaks-over-threshold method and the annual maximum method for flood frequency analysis. *Hydrol. Sci. J.* 59, 959–977. <https://doi.org/10.1080/02626667.2013.831174>.
- Bischiotti, K., van den Hurk, B., Jongman, B., Coughlan de Perez, E., Veldkamp, T., de Moel, H., Aerts, J., 2018. The influence of antecedent conditions on flood risk in sub-Saharan Africa. *Nat. Hazards Earth Syst. Sci.* 18, 271–285. <https://doi.org/10.5194/nhess-18-271-2018>.
- Blöschl, G., Merz, R., Reszler, C., 2007. FLOODS IN AUSTRIA, in: *Extreme Hydrological Events: New Concepts for Security*. Springer Netherlands, Dordrecht, pp. 81–90. 10.1007/978-1-4020-5741-0_6.
- Blöschl, G., Hall, J., Parajka, J., Perdigão, R.A.P., Merz, B., Arheimer, B., Aronica, G.T., Bilibashi, A., Bonacci, O., Borga, M., Canjevac, I., Castellarin, A., Chirico, G.B., Claps,

- P., Fiala, K., Frolova, N., Gorbachova, L., Gül, A., Hannaford, J., Harrigan, S., Kireeva, M., Kiss, A., Kjeldsen, T.R., Kohnová, S., Koskela, J.J., Ledvinka, O., Macdonald, N., Mavrova-Guirguinova, M., Mediero, L., Merz, R., Molnar, P., Montanari, A., Murphy, C., Osuch, M., Ovcharuk, V., Radevski, I., Rogger, M., Salinas, J.L., Sauquet, E., Šraj, M., Szolgay, J., Viglione, A., Volpi, E., Wilson, D., Zaimi, K., Živković, N., 2017. Changing climate shifts timing of European floods. *Science* (80-). 357, 588–590. <https://doi.org/10.1126/science.aan2506>.
- Blöschl, G., Hall, J., Viglione, A., Perdigão, R.A.P., Parajka, J., Merz, B., Lun, D., Arheimer, B., Aronica, G.T., Bilibashi, A., Boháč, M., Bonacci, O., Borgia, M., Canjevac, I., Castellarin, A., Chirico, G.B., Claps, P., Frolova, N., Ganora, D., Gorbachova, L., Gül, A., Hannaford, J., Harrigan, S., Kireeva, M., Kiss, A., Kjeldsen, T.R., Kohnová, S., Koskela, J.J., Ledvinka, O., Macdonald, N., Mavrova-Guirguinova, M., Mediero, L., Merz, R., Molnar, P., Montanari, A., Murphy, C., Osuch, M., Ovcharuk, V., Radevski, I., Salinas, J.L., Sauquet, E., Šraj, M., Szolgay, J., Volpi, E., Wilson, D., Zaimi, K., Živković, N., 2019. Changing climate both increases and decreases European river floods. *Nature* 573, 108–111. <https://doi.org/10.1038/s41586-019-1495-6>.
- Bonaccorso, B., Peres, D.J., Cancelliere, A., Rossi, G., 2013. Large scale probabilistic drought characterization over Europe. *Water Resour. Manag.* 27, 1675–1692. <https://doi.org/10.1007/s11269-012-0177-z>.
- Brázdil, R., Kundzewicz, Z.W., Benito, G., 2006. Historical hydrology for studying flood risk in Europe. *Hydrol. Sci. J.* 51, 739–764. <https://doi.org/10.1623/hysj.51.5.739>.
- Brimelow, J.C., Hanesiak, J.M., Burrows, W.R., 2011. Impacts of land-atmosphere feedbacks on deep, moist convection on the Canadian prairies. *Earth Interact.* 15 <https://doi.org/10.1175/2011EI407.1>.
- Brocca, L., Ponzi, F., Moramarco, T., Melone, F., Berni, N., Wagner, W., 2012. Improving landslide forecasting using ASCAT-derived soil moisture data: a case study of the Torgioannetto Landslide in Central Italy. *Remote Sens.* 4, 1232–1244. <https://doi.org/10.3390/rs4051232>.
- Christopoulos, S.R.G., Skordas, E.S., Sarlis, N.V., 2020. On the statistical significance of the variability minima of the order parameter of seismicity by means of event coincidence analysis. *Appl. Sci.* 10 <https://doi.org/10.3390/app10020662>.
- Cornes, R.C., van der Schrier, G., van den Besselaar, E.J.M., Jones, P.D., 2018. An Ensemble Version of the E-OBS Temperature and Precipitation Data Sets. *J. Geophys. Res.* 123, 9391–9409. <https://doi.org/10.1029/2017JD028200>.
- Coumou, D., Rahmstorf, S., 2012. A decade of weather extremes. *Nat. Clim. Chang.* 2, 491–496. <https://doi.org/10.1038/nclimate1452>.
- Di Sante, F., Coppola, E., Giorgi, F., 2021. Projections of river floods in Europe using EURO-CORDEX, CMIP5 and CMIP6 simulations. *Int. J. Climatol.* 41, 3203–3221. <https://doi.org/10.1002/joc.7014>.
- Dietze, M., Bell, R., Ozturk, U., Cook, K.L., Andermann, C., Beer, A.R., Damm, B., Lucia, A., Fauer, F.S., Nissen, K.M., Sieg, T., Thieken, A.H., 2022. More than heavy rain turning into fast-flowing water – a landscape perspective on the 2021 Eifel floods. *Nat. Hazards Earth Syst. Sci.* 22, 1845–1856. <https://doi.org/10.5194/nhess-22-1845-2022>.
- Do, H.X., Westra, S., Leonard, M., 2017. A global-scale investigation of trends in annual maximum streamflow. *J. Hydrol.* 552, 28–43. <https://doi.org/10.1016/j.jhydrol.2017.06.015>.
- Donges, J.F., Donner, R.V., Trauth, M.H., Marwan, N., Schellnhuber, H.J., Kurths, J., 2011. Nonlinear detection of paleoclimate-variability transitions possibly related to human evolution. *Proc. Natl. Acad. Sci. U. S. A.* 108, 20422–20427. <https://doi.org/10.1073/pnas.1117052108>.
- Donges, J.F., Schleussner, C.-F., Siegmund, J.F., Donner, R.V., 2016. Event coincidence analysis for quantifying statistical interrelationships between event time series. *Eur. Phys. J. Spec. Top.* 225, 471–487. <https://doi.org/10.1140/epjst/e2015-50233-y>.
- Dottori, F., Mentaschi, L., Bianchi, A., Alfieri, L., Feyen, L., 2023. Cost-effective adaptation strategies to rising river flood risk in Europe. *Nat. Clim. Chang.* 10.1038/s41558-022-01540-0.
- Fdez-Arroyabe, P., Formeilles-Callejón, J., Santurtún, A., Szangolies, L., Donner, R.V., 2020. Schumann resonance and cardiovascular hospital admission in the area of Granada, Spain: an event coincidence analysis approach. *Sci. Total Environ.* 705, 135813 <https://doi.org/10.1016/j.scitotenv.2019.135813>.
- Froidevaux, P., Schwanbeck, J., Weingartner, R., Chevalier, C., Martius, O., 2015. Flood triggering in Switzerland: The role of daily to monthly preceding precipitation. *Hydrol. Earth Syst. Sci.* 19, 3903–3924. <https://doi.org/10.5194/hess-19-3903-2015>.
- Garg, S., Mishra, V., 2019. Role of extreme precipitation and initial hydrologic conditions on floods in Godavari River Basin, India. *Water Resour. Res.* 55, 9191–9210. <https://doi.org/10.1029/2019WR025863>.
- Gervais, M., Tremblay, L.B., Gyakum, J.R., Atallah, E., 2014. Representing extremes in a daily gridded precipitation analysis over the United States: impacts of station density, resolution, and gridding methods. *J. Clim.* 27, 5201–5218. <https://doi.org/10.1175/JCLI-D-13-00319.1>.
- Ghajarina, N., Kalantari, Z., Orth, R., Destouni, G., 2020. Close co-variation between soil moisture and runoff emerging from multi-catchment data across Europe. *Sci. Rep.* 10, 4817. <https://doi.org/10.1038/s41598-020-61621-y>.
- Good, S.P., Moore, G.W., Miralles, D.G., 2017. A mesic maximum in biological water use separates biome sensitivity to aridity shifts. *Nat. Ecol. Evol.* 1, 1883–1888. <https://doi.org/10.1038/s41559-017-0371-8>.
- Grabowska, K., 2008. Storms in Europe (1994–2005) – their relationship with continentality of climate. *Misc. Geogr.* 13, 67–75. <https://doi.org/10.2478/mgrsd-2008-0007>.
- Grillakis, M.G., Koutroulis, A.G., Komma, J., Tsanis, I.K., Wagner, W., Blöschl, G., 2016. Initial soil moisture effects on flash flood generation – a comparison between basins of contrasting hydro-climatic conditions. *J. Hydrol.* 541, 206–217. <https://doi.org/10.1016/j.jhydrol.2016.03.007>.
- Gu, X., Zhang, Q., Li, J., Chen, D., Singh, V.P., Zhang, Y., Liu, J., Shen, Z., Yu, H., 2020. Impacts of anthropogenic warming and uneven regional socio-economic development on global river flood risk. *J. Hydrol.* 590, 125262 <https://doi.org/10.1016/j.jhydrol.2020.125262>.
- Guilod, B.P., Orlowsky, B., Miralles, D.G., Teuling, A.J., Seneviratne, S.I., 2015. Reconciling spatial and temporal soil moisture effects on afternoon rainfall. *Nat. Commun.* 6, 6443. <https://doi.org/10.1038/ncomms7443>.
- Guntur, R.K., Maheswaran, R., Agarwal, A., Singh, V.P., 2020. Accounting for temporal variability for improved precipitation regionalization based on self-organizing map coupled with information theory. *J. Hydrol.* 590, 125236 <https://doi.org/10.1016/j.jhydrol.2020.125236>.
- Hall, J., Blöschl, G., 2018. Spatial patterns and characteristics of flood seasonality in Europe. *Hydrol. Earth Syst. Sci.* 22, 3883–3901. <https://doi.org/10.5194/hess-22-3883-2018>.
- Hall, J., Arheimer, B., Aronica, G.T., Bilibashi, A., Boháč, M., Bonacci, O., Borgia, M., Burlando, P., Castellarin, A., Chirico, G.B., Claps, P., Fiala, K., Gaál, L., Gorbachova, L., Gül, A., Hannaford, J., Kiss, A., Kjeldsen, T., Kohnová, S., Koskela, J.J., MacDonald, N., Mavrova-Guirguinova, M., Ledvinka, O., Mediero, L., Merz, B., Merz, R., Molnar, P., Montanari, A., Osuch, M., Parajka, J., Perdigão, R.A.P., Radevski, I., Renard, B., Rogger, M., Salinas, J.L., Sauquet, E., Šraj, M., Szolgay, J., Viglione, A., Volpi, E., Wilson, D., Zaimi, K., Blöschl, G., 2015. A European flood database: Facilitating comprehensive flood research beyond administrative boundaries, in: IAHS-AISH Proceedings and Reports. Copernicus GmbH, pp. 89–95. 10.5194/piahs-370-89-2015.
- Hannaford, J., Lloyd-Hughes, B., Keef, C., Parry, S., Prudhomme, C., 2011. Examining the large-scale spatial coherence of European drought using regional indicators of precipitation and streamflow deficit. *Hydrol. Process.* 25, 1146–1162. <https://doi.org/10.1002/hyp.7725>.
- Hänsel, S., Ustrnul, Z., Lupikasza, E., Skalák, P., 2019. Assessing seasonal drought variations and trends over Central Europe. *Adv. Water Resour.* 127, 53–75. <https://doi.org/10.1016/j.advwatres.2019.03.005>.
- Harris, P.P., Folwell, S.S., Gallego-Elvira, B., Rodríguez, J., Milton, S., Taylor, C.M., 2017. An evaluation of modeled evaporation regimes in Europe using observed dry spell land surface temperature. *J. Hydrometeorol.* 18, 1453–1470. <https://doi.org/10.1175/JHM-D-16-0227.1>.
- Haylock, M.R., Hofstra, N., Klein Tank, A.M.G., Klok, E.J., Jones, P.D., New, M., 2008. A European daily high-resolution gridded data set of surface temperature and precipitation for 1950–2006. *J. Geophys. Res.* 113, D20119. <https://doi.org/10.1029/2008JD010201>.
- He, X., Sheffield, J., 2020. Lagged compound occurrence of droughts and pluvials globally over the past seven decades. *Geophys. Res. Lett.* 47 <https://doi.org/10.1029/2020GL087924>.
- Hlavcova, K., Kohnova, S., Kubes, R., Szolgay, J., Zvolensky, M., 2005. An empirical method for estimating future flood risks for flood warnings. *Hydrol. Earth Syst. Sci.* 9, 431–448. <https://doi.org/10.5194/hess-9-431-2005>.
- Hu, G., Franzke, C.L.E., 2020. Evaluation of daily precipitation extremes in reanalysis and gridded observation-based data sets over Germany. *Geophys. Res. Lett.* 47 <https://doi.org/10.1029/2020GL089624>.
- Hundeche, Y., Parajka, J., Viglione, A., 2020. Assessment of past flood changes across Europe based on flood-generating processes. *Hydrol. Sci. J.* 65, 1830–1847. <https://doi.org/10.1080/02626667.2020.1782413>.
- Ibeuchi, C.C., 2022. Patterns of atmospheric circulation in Western Europe linked to heavy rainfall in Germany: preliminary analysis into the 2021 heavy rainfall episode. *Theor. Appl. Climatol.* 148, 269–283. <https://doi.org/10.1007/s00704-022-03945-5>.
- IPCC, 2021. Assessment Report 6 Climate Change 2021: The Physical Science Basis.
- Iturbide, M., Gutiérrez, J.M., Alves, L.M., Bedia, J., Cima-de-ville, E., Cofiño, A., Cerezo-Mota, R., Di Luca, A., Faria, S.H., Gorodetskaya, I., Hauser, M., Herrera, S., Hewitt, H., Hennessy, K., Jones, R., Krakovska, S., Manzanas, R., Martínez-Castro, D., Narisma, G.T., Nurhati, I., Pinto, I., Seneviratne, S., van den Hurk, B., Vera, C., 2020. An update of IPCC climate reference regions for subcontinental analysis of climate model data: Definition and aggregated datasets. *Earth Syst. Sci. Data Discuss.* 1–16 <https://doi.org/10.5194/essd-2019-258>.
- Jaeger, E.B., Seneviratne, S.I., 2011. Impact of soil moisture-atmosphere coupling on European climate extremes and trends in a regional climate model. *Clim. Dyn.* 36, 1919–1939. <https://doi.org/10.1007/s00382-010-0780-8>.
- Jiang, Y., Cooley, D., Wehner, M.F., 2020. Principal component analysis for extremes and application to U.S. precipitation. *J. Clim.* 33, 6441–6451. <https://doi.org/10.1175/JCLI-D-19-0413.1>.
- Jongman, B., Hochrainer-Stigler, S., Feyen, L., Aerts, J.C.J.H., Mechler, R., Botzen, W.J.W., Bouwer, L.M., Pflug, G., Rojas, R., Ward, P.J., 2014. Increasing stress on disaster-risk finance due to large floods. *Nat. Clim. Chang.* 4, 264–268. <https://doi.org/10.1038/nclimate2124>.
- Kam, P.M., Aznar-Siguan, G., Schewe, J., Milano, L., Ginnett, J., Willner, S., McCaughey, J.W., Bresch, D.N., 2021. Global warming and population change both heighten future risk of human displacement due to river floods. *Environ. Res. Lett.* 16 <https://doi.org/10.1088/1748-9326/abd26c>.
- Kemter, M., Merz, B., Marwan, N., Vorogushyn, S., Blöschl, G., 2020. Joint trends in flood magnitudes and spatial extents across Europe. *Geophys. Res. Lett.* 47, 1–8. <https://doi.org/10.1029/2020GL087464>.
- Kemter, M., Fischer, M., Luna, L.V., Schönfeldt, E., Vogel, J., Banerjee, A., Korup, O., Thonicke, K., 2021. Cascading hazards in the aftermath of Australia's 2019/2020 Black Summer wildfires. *Earth's Futur.* 1–7 <https://doi.org/10.1029/2020ef001884>.
- Khatun, A., Ganguli, P., Bisht, D.S., Chatterjee, C., Sahoo, B., 2022. Understanding the impacts of predecessor rain events on flood hazard in a changing climate. *Hydrol. Process.* <https://doi.org/10.1002/hyp.14500>.

- Klein Tank, A.M.G., Wijngaard, J.B., Können, G.P., Böhm, R., Demarée, G., Gocheva, A., Milet, M., Pashiardis, S., Hejkrlik, L., Kern-Hansen, C., Heino, R., Bessemoulin, P., Müller-Westermeier, G., Tzanakou, M., Szalai, S., Páldóttir, T., Fitzgerald, D., Rubin, S., Capaldo, M., Maugeri, M., Leitass, A., Bukantis, A., Aberfeld, R., van Engelen, A.F.V., Forland, E., Miletus, M., Coelho, F., Mares, C., Razuvaev, V., Nieplova, E., Cegnar, T., Antonio López, J., Dahlström, B., Moberg, A., Kirchhofer, W., Ceylan, A., Pachaliuk, O., Alexander, L.V., Petrovic, P., 2002. Daily dataset of 20th-century surface air temperature and precipitation series for the European Climate Assessment. *Int. J. Climatol.* 22, 1441–1453. <https://doi.org/10.1002/joc.773>.
- Klok, E.J., Klein Tank, A.M.G., 2009. Updated and extended European dataset of daily climate observations. *Int. J. Climatol.* 29, 1182–1191. <https://doi.org/10.1002/joc.1779>.
- Komma, J., Blöschl, G., Reszler, C., 2008. Soil moisture updating by Ensemble Kalman Filtering in real-time flood forecasting. *J. Hydrol.* 357, 228–242. <https://doi.org/10.1016/j.jhydrol.2008.05.020>.
- Koster, R.D., Guo, Z., Yang, R., Dirmeyer, P.A., Mitchell, K., Puma, M.J., 2009. On the nature of soil moisture in land surface models. *J. Clim.* 22, 4322–4335. <https://doi.org/10.1175/2009JCLI2832.1>.
- Kostopoulou, E., Giannakopoulos, C., Hatzaki, M., Tziotziou, K., 2012. Climate extremes in the NE Mediterranean: Assessing the E-OBS dataset and regional climate simulations. *Clim. Res.* 54, 249–270. <https://doi.org/10.3354/cr01110>.
- Leckebusch, G.C., Ulbrich, U., 2004. On the relationship between cyclones and extreme windstorm events over Europe under climate change. *Glob. Planet. Change* 44, 181–193. <https://doi.org/10.1016/j.gloplacha.2004.06.011>.
- Leonard, M., Westra, S., Phatak, A., Lambert, M., van den Hurk, B., McInnes, K., Risbey, J., Schuster, S., Jakob, D., Stafford-Smith, M., 2014. A compound event framework for understanding extreme impacts. *Wiley Interdiscip. Rev. Clim. Chang.* 5, 113–128. <https://doi.org/10.1002/wcc.252>.
- Lun, D., Viglione, A., Bertola, M., Komma, J., Parajka, J., Valent, P., Blöschl, G., 2021. Characteristics and process controls of statistical flood moments in Europe - a data-based analysis. *Hydrol. Earth Syst. Sci.* 25, 5535–5560. <https://doi.org/10.5194/hess-25-5535-2021>.
- Madsen, H., Lawrence, D., Lang, M., Martinkova, M., Kjeldsen, T.R., 2014. Review of trend analysis and climate change projections of extreme precipitation and floods in Europe. *J. Hydrol.* 519, 3634–3650. <https://doi.org/10.1016/j.jhydrol.2014.11.003>.
- Manoj, J.A., Guntu, R.K., Agarwal, A., 2022. Spatiotemporal dependence of soil moisture and precipitation over India. *J. Hydrol.* 610, 127898 <https://doi.org/10.1016/j.jhydrol.2022.127898>.
- Martens, B., Miralles, D.G., Lievens, H., van der Schalie, R., de Jeu, R.A.M., Fernández-Prieto, D., Beck, H.E., Dorigo, W.A., Verhoest, N.E.C., 2017. GLEAM v3: satellite-based land evaporation and root-zone soil moisture. *Geosci. Model Dev.* 10, 1903–1925. <https://doi.org/10.5194/gmd-10-1903-2017>.
- Massari, C., Camici, S., Ciabatta, L., Brocca, L., 2018. Exploiting satellite-based surface soil moisture for flood forecasting in the Mediterranean area: State update versus rainfall correction. *Remote Sens.* 10 <https://doi.org/10.3390/rs10020292>.
- McDonnell, J.J., Woods, R., 2004. On the need for catchment classification. *J. Hydrol.* 299, 2–3. <https://doi.org/10.1016/j.jhydrol.2004.09.003>.
- Mediero, L., Santillán, D., Garrote, L., Granados, A., 2014. Detection and attribution of trends in magnitude, frequency and timing of floods in Spain. *J. Hydrol.* 517, 1072–1088. <https://doi.org/10.1016/j.jhydrol.2014.06.040>.
- Mediero, L., Kjeldsen, T.R., Macdonald, N., Kohnova, S., Merz, B., Vorogushyn, S., Wilson, D., Alburquerque, T., Blöschl, G., Bogdanowicz, E., Castellari, A., Hall, J., Kobold, M., Kriauciuniene, J., Lang, M., Madsen, H., Onuslu, G., Perdigão, R.A.P., Roald, L.A., Salinas, J.L., Toumazis, A.D., Veijalainen, N., Órarninnsson, Ó., 2015. Identification of coherent flood regions across Europe by using the longest streamflow records. *J. Hydrol.* 528, 341–360. <https://doi.org/10.1016/j.jhydrol.2015.06.016>.
- Merz, R., Blöschl, G., 2008. Flood frequency hydrology: 1. Temporal, spatial, and causal expansion of information. *Water Resour. Res.* 44, 1–17. <https://doi.org/10.1029/2007WR006744>.
- Merz, B., Blöschl, G., Vorogushyn, S., Dottori, F., Aerts, J.C.J.H., Bates, P., Bertola, M., Kemter, M., Kreibich, H., Lall, U., Macdonald, E., 2021. Causes, impacts and patterns of disastrous river floods, 0123456789 *Nat. Rev. Earth Environ.* <https://doi.org/10.1038/s43017-021-00195-3>.
- Mikolaskova, K., 2009. Continental and oceanic precipitation regime in Europe. *Open Geosci.* 1 <https://doi.org/10.2478/v10085-009-0013-8>.
- Miralles, D.G., Holmes, T.R.H., De Jeu, R.A.M., Gash, J.H., Meesters, A.G.C.A., Dolman, A.J., 2011. Global land-surface evaporation estimated from satellite-based observations. *Hydrol. Earth Syst. Sci.* 15, 453–469. <https://doi.org/10.5194/hess-15-453-2011>.
- Miralles, D.G., Teuling, A.J., van Heerwaarden, C.C., Vilà-Guerau de Arellano, J., 2014. Mega-heatwave temperatures due to combined soil desiccation and atmospheric heat accumulation. *Nat. Geosci.* 7, 345–349. <https://doi.org/10.1038/ngeo2141>.
- Mishra, A., Mukherjee, S., Merz, B., Singh, V.P., Wright, D.B., Villari, G., Paul, S., Kumar, D.N., Khedun, C.P., Niyogi, D., Schumann, G., Stedinger, J.R., 2022. An overview of flood concepts, challenges, and future directions. *J. Hydrol. Eng.* 27, 1–30. [https://doi.org/10.1061/\(asce\)jhe.1943-5584.0002164](https://doi.org/10.1061/(asce)jhe.1943-5584.0002164).
- Moghimi, S., Teuling, A.J., Uijlenhoet, R., 2022. A probabilistic climate change assessment for Europe. *Int. J. Climatol.* 1–17 <https://doi.org/10.1002/joc.7604>.
- Mondal, S., Mishra, A.K., Leung, L.R., 2020. Spatiotemporal characteristics and propagation of summer extreme precipitation events over United States: a complex network analysis. *Geophys. Res. Lett.* 47 <https://doi.org/10.1029/2020GL088185>.
- Nistor, M.-M., Man, T.C., Benzaghta, M.A., Nedumpallile Vasu, N., Dezsi, S., Kizza, R., 2018. Land cover and temperature implications for the seasonal evapotranspiration in Europe. *Geogr. Tech.* 13, 39–50. <https://doi.org/10.21163/GT.2018.131.09>.
- Pall, P., Allen, M.R., Stone, D.A., 2007. Testing the Clausius-Clapeyron constraint on changes in extreme precipitation under CO2 warming. *Clim. Dyn.* 28, 351–363. <https://doi.org/10.1007/s00382-006-0180-2>.
- Papalexio, S.M., Montanari, A., 2019. Global and regional increase of precipitation extremes under global warming. *Water Resour. Res.* 55, 4901–4914. <https://doi.org/10.1029/2018WR024067>.
- Peel, M.C., Finlayson, B.L., McMahon, T.A., 2007. Updated world map of the Köppen-Geiger climate classification. *Hydrol. Earth Syst. Sci.* 11, 1633–1644. <https://doi.org/10.5194/hess-11-1633-2007>.
- Pendergrass, A.G., 2018. What precipitation is extreme? *Science* (80-) 360, 1072–1073. <https://doi.org/10.1126/science.aat1871>.
- Pérez Ciria, T., Chiogna, G., 2020. Intra-catchment comparison and classification of long-term streamflow variability in the Alps using wavelet analysis. *J. Hydrol.* 587, 124927 <https://doi.org/10.1016/j.jhydrol.2020.124927>.
- Pérez Ciria, T., Labat, D., Chiogna, G., 2019. Detection and interpretation of recent and historical streamflow alterations caused by river damming and hydropower production in the Adige and Inn river basins using continuous, discrete and multiresolution wavelet analysis. *J. Hydrol.* 578, 124021 <https://doi.org/10.1016/j.jhydrol.2019.124021>.
- Pyarali, K., Peng, J., Disse, M., Tuo, Y., 2022. Development and application of high resolution SPEI drought dataset for Central Asia. *Sci. Data* 9, 172. <https://doi.org/10.1038/s41597-022-01279-5>.
- R Core Team, 2021. R: A Language and Environment for Statistical Computing.
- Ray, R.L., Jacobs, J.M., 2007. Relationships among remotely sensed soil moisture, precipitation and landslide events. *Nat. Hazards* 43, 211–222. <https://doi.org/10.1007/s11069-006-9095-9>.
- Schär, C., Lüthi, D., Beyerle, U., Heise, E., 1999. The soil-precipitation feedback: a process study with a regional climate model. *J. Clim.* 12, 722–741. [https://doi.org/10.1175/1520-0442\(1999\)012<0722:TSPFAP>2.0.CO;2](https://doi.org/10.1175/1520-0442(1999)012<0722:TSPFAP>2.0.CO;2).
- Schröter, K., Kunz, M., Elmer, F., Mühr, B., Merz, B., 2015. What made the June 2013 flood in Germany an exceptional event? A hydro-meteorological evaluation. *Hydrol. Earth Syst. Sci.* 19, 309–327. <https://doi.org/10.5194/hess-19-309-2015>.
- Schulzweida, U., 2019. CDO User Guide 1–206.
- Schumacher, D.L., Keune, J., van Heerwaarden, C.C., Vilà-Guerau de Arellano, J., Teuling, A.J., Miralles, D.G., 2019. Amplification of mega-heatwaves through heat torrents fuelled by upwind drought. *Nat. Geosci.* 12, 712–717. <https://doi.org/10.1038/s41561-019-0431-6>.
- Schwingshackl, C., Hirschi, M., Seneviratne, S.I., 2017. Quantifying spatiotemporal variations of soil moisture control on surface energy balance and near-surface air temperature. *J. Clim.* 30, 7105–7124. <https://doi.org/10.1175/JCLI-D-16-0727.1>.
- Seneviratne, S.I., Lüthi, D., Litschi, M., Schär, C., 2006. Land-atmosphere coupling and climate change in Europe. *Nature* 443, 205–209. <https://doi.org/10.1038/nature05095>.
- Seneviratne, S.I., Corti, T., Davin, E.L., Hirschi, M., Jaeger, E.B., Lehner, I., Orlowsky, B., Teuling, A.J., 2010. Investigating soil moisture–climate interactions in a changing climate: a review. *Earth-Sci. Rev.* 99, 125–161. <https://doi.org/10.1016/j.earscirev.2010.02.004>.
- Seneviratne, S.I., Nicholls, N., Easterling, D., Goodess, C.M., Kanae, S., Kossin, J., Luo, Y., Marengo, J., McInnes, K., Rahimi, M., Reichstein, M., Sorteberg, A., Vera, C., Zhang, X., Rusticucci, M., Semenov, V., Alexander, L. V., Allen, S., Benito, G., Cavazos, T., Clague, J., Conway, D., Della-Marta, P.M., Gerber, M., Gong, S., Goswami, B.N., Hemer, M., Huggel, C., van den Hurk, B., Khari, V. V., Kitoh, A., Tank, A.M.G.K., Li, G., Mason, S., McGuire, W., van Oldenborgh, G.J., Orlowsky, B., Smith, S., Thiaw, W., Velegakis, A., Yiou, P., Zhang, T., Zhou, T., Zwiers, F.W., 2012. Changes in Climate Extremes and their Impacts on the Natural Physical Environment, in: Field, C.B., Barros, V., Stocker, T.F., Dahe, Q. (Eds.), *Managing the Risks of Extreme Events and Disasters to Advance Climate Change Adaptation*. Cambridge University Press, Cambridge, pp. 109–230. <https://doi.org/10.1017/CBO9781139177245.006>.
- Seneviratne, S.I., Zhang, X., Adnan, M., Badi, W., Dereczynski, C., Luca, A. Di, Ghosh, S., Iskandar, I., Kossin, J., Lewis, S., Otto, F., Pinto, I., Satoh, M., Vicente-Serrano, S.M., Wehner, M., Zhou, B., 2021. Weather and Climate Extreme Events in a Changing Climate. In: *Climate Change 2021: The Physical Science Basis. Contribution of Working Group I to the Sixth Assessment Report of the Intergovernmental Panel on Climate Change*. *Clim. Chang.* 2021 Phys. Sci. Basis. Contrib. Work. Gr. I to Sixth Assess. Rep. Intergov. Panel Clim. Chang. 366.
- Sharma, A., Wasko, C., Lettenmaier, D.P., 2018. If precipitation extremes are increasing, why aren't floods? *Water Resour. Res.* 54, 8545–8551. <https://doi.org/10.1029/2018WR023749>.
- Sheridan, S.C., Lee, C.C., 2018. Temporal trends in absolute and relative extreme temperature events across North America. *J. Geophys. Res. Atmos.* 123, 11889–11898. <https://doi.org/10.1029/2018JD029150>.
- Siegmund, J.F., Sanders, T.G.M., Heinrich, I., Van Der Maaten, E., Simard, S., Helle, G., Donner, R.V., 2016a. Meteorological drivers of extremes in daily stem radius variations of beech, oak, and pine in Northeastern Germany: an event coincidence analysis. *Front. Plant Sci.* 7 <https://doi.org/10.3389/fpls.2016.00733>.
- Siegmund, J.F., Wiedermann, M., Donges, J.F., Donner, R.V., 2016b. Impact of temperature and precipitation extremes on the flowering dates of four German wildlife shrub species. *Biogeosciences* 13, 5541–5555. <https://doi.org/10.5194/bg-13-5541-2016>.
- Siegmund, J.F., Siegmund, N., Donner, R.V., 2017. CoinCalc—a new R package for quantifying simultaneities of event series. *Comput. Geosci.* 98, 64–72. <https://doi.org/10.1016/j.cageo.2016.10.004>.
- Sun, A.Y., Scanlon, B.R., AghaKouchak, A., Zhang, Z., 2017. Using GRACE satellite gravimetry for assessing large-scale hydrologic extremes. *Remote Sens.* 9 <https://doi.org/10.3390/rs9121287>.

- Sun, A.Y., Xia, Y., Caldwell, T.G., Hao, Z., 2018. Patterns of precipitation and soil moisture extremes in Texas, US: a complex network analysis. *Adv. Water Resour.* 112, 203–213. <https://doi.org/10.1016/j.advwatres.2017.12.019>.
- Taesombut, V., Yevjevich, V., 1978. Use of Partial Flood Series for Estimating Distribution of Maximum Annual Flood Peak. Colo State Univ (Fort Collins) Hydrol Pap.
- Tallaksen, L.M., Stahl, K., 2014. Spatial and temporal patterns of large-scale droughts in Europe: Model dispersion and performance. *Geophys. Res. Lett.* 41, 429–434. <https://doi.org/10.1002/2013GL058573>.
- Templ, B., Templ, M., Barbieri, R., Meier, M., Zufferey, V., 2021. Coincidence of temperature extremes and phenological events of grapevines. *Oeno One* 55, 367–383. <https://doi.org/10.20870/OENO-ONE.2021.55.1.3187>.
- Teuling, A.J., Hirschi, M., Ohmura, A., Wild, M., Reichstein, M., Ciais, P., Buchmann, N., Ammann, C., Montagnani, L., Richardson, A.D., Wohlfahrt, G., Seneviratne, S.I., 2009. A regional perspective on trends in continental evaporation. *Geophys. Res. Lett.* 36, n/a-n/a. <https://doi.org/10.1029/2008GL036584>.
- Thompson, R., 1995. Complex demodulation and the estimation of the changing continentality of Europe's climate. *Int. J. Climatol.* 15, 175–185. <https://doi.org/10.1002/joc.3370150204>.
- Timmermans, B., Wehner, M., Cooley, D., O'Brien, T., Krishnan, H., 2019. An evaluation of the consistency of extremes in gridded precipitation data sets. *Clim. Dyn.* 52, 6651–6670. <https://doi.org/10.1007/s00382-018-4537-0>.
- Wasko, C., Nathan, R., 2019. Influence of changes in rainfall and soil moisture on trends in flooding. *J. Hydrol.* 575, 432–441. <https://doi.org/10.1016/j.jhydrol.2019.05.054>.
- Wasko, C., Nathan, R., Peel, M.C., 2020. Changes in antecedent soil moisture modulate flood seasonality in a changing climate. *Water Resour. Res.* 56 <https://doi.org/10.1029/2019WR026300>.
- Wasko, C., Nathan, R., Stein, L., O'Shea, D., 2021. Evidence of shorter more extreme rainfalls and increased flood variability under climate change. *J. Hydrol.* 603, 126994 <https://doi.org/10.1016/j.jhydrol.2021.126994>.
- Westra, S., Alexander, L.V., Zwiers, F.W., 2013. Global increasing trends in annual maximum daily precipitation. *J. Clim.* 26, 3904–3918. <https://doi.org/10.1175/JCLI-D-12-00502.1>.
- Wiedermann, M., Siegmund, J.F., Donges, J.F., Donner, R.V., 2021. Differential imprints of distinct ENSO flavors in global patterns of very low and high seasonal precipitation. *Front. Clim.* 3, 1–14. <https://doi.org/10.3389/fclim.2021.618548>.
- Wolf, F., Ozturk, U., Cheung, K., Donner, R.V., 2021. Spatiotemporal patterns of synchronous heavy rainfall events in East Asia during the Baiu season. *Earth Syst. Dyn.* 12, 295–312. <https://doi.org/10.5194/esd-12-295-2021>.
- Xing, Z., Yu, Z., Wei, J., Zhang, X., Ma, M., Yi, P., Ju, Q., Wang, J., Laux, P., Kunstmann, H., 2022. Lagged influence of ENSO regimes on droughts over the Poyang Lake basin. *China. Atmos. Res.* 275, 106218 <https://doi.org/10.1016/j.atmosres.2022.106218>.
- Zanardo, S., Nicotina, L., Hilberts, A.G.J., Jewson, S.P., 2019. Modulation of Economic Losses From European Floods by the North Atlantic Oscillation. *Geophys. Res. Lett.* 46, 2563–2572. <https://doi.org/10.1029/2019GL081956>.
- Zehe, E., Blöschl, G., 2004. Predictability of hydrologic response at the plot and catchment scales: Role of initial conditions. *Water Resour. Res.* 40, 1–21. <https://doi.org/10.1029/2003WR002869>.
- Zhai, X., Guo, L., Liu, R., Zhang, Y., 2018. Rainfall threshold determination for flash flood warning in mountainous catchments with consideration of antecedent soil moisture and rainfall pattern. *Nat. Hazards* 94, 605–625. <https://doi.org/10.1007/s11069-018-3404-y>.
- Zhang, W., Villarini, G., 2020. Deadly compound heat stress-flooding hazard across the Central United States. *Geophys. Res. Lett.* 47, 1–7. <https://doi.org/10.1029/2020GL089185>.
- Zscheischler, J., Martius, O., Westra, S., Bevacqua, E., Raymond, C., Horton, R.M., van den Hurk, B., Aghakouchak, A., Jézéquel, A., Mahecha, M.D., Maraun, D., Ramos, A. M., Ridder, N.N., Thiery, W., Vignotto, E., 2020. A typology of compound weather and climate events. *Nat. Rev. Earth Environ.* 1, 333–347. <https://doi.org/10.1038/s43017-020-0060-z>.
- Zscheischler, J., Seneviratne, S.I., 2017. Dependence of drivers affects risks associated with compound events. *Sci. Adv.* 3 <https://doi.org/10.1126/sciadv.1700263>.
- Zscheischler, J., Westra, S., Van Den Hurk, B.J.J.M., Seneviratne, S.I., Ward, P.J., Pitman, A., Aghakouchak, A., Bresch, D.N., Leonard, M., Wahl, T., Zhang, X., 2018. Future climate risk from compound events. *Nat. Clim. Chang.* 8, 469–477. <https://doi.org/10.1038/s41558-018-0156-3>.